Mon. Not. R. Astron. Soc. **000**, 1–30 (2013) Printed 27 August 2014 (MN LATEX style file v2.2)

The evolution of the star forming sequence in hierarchical galaxy formation models

Peter D. Mitchell⋆, Cedric G. Lacey, Shaun Cole, Carlton M. Baugh

Institute for Computational Cosmology, Department of Physics, University of Durham, South Road, Durham, DH1 3LE, UK.

27 August 2014

arXiv:1403.1585v2 [astro-ph.CO] 26 Aug 2014

ABSTRACT

It has been argued that the specific star formation rates of star forming galaxies inferred from observational data decline more rapidly below $z = 2$ than is predicted by hierarchical galaxy formation models. We present a detailed analysis of this problem by comparing predictions from the GALFORM semi-analytic model with an extensive compilation of data on the average star formation rates of star-forming galaxies. We also use this data to infer the form of the stellar mass assembly histories of star forming galaxies. Our analysis reveals that the currently available data favour a scenario where the stellar mass assembly histories of star forming galaxies rise at early times and then fall towards the present day. In contrast, our model predicts stellar mass assembly histories that are almost flat below $z = 2$ for star forming galaxies, such that the predicted star formation rates can be offset with respect to the observational data by factors of up to $2 - 3$. This disagreement can be explained by the level of coevolution between stellar and halo mass assembly that exists in contemporary galaxy formation models. In turn, this arises because the standard implementations of star formation and supernova feedback used in the models result in the efficiencies of these process remaining approximately constant over the lifetime of a given star forming galaxy. We demonstrate how a modification to the timescale for gas ejected by feedback to be reincorporated into galaxy haloes can help to reconcile the model predictions with the data.

Key words: galaxies: formation – galaxies: evolution – galaxies: star formation

1 INTRODUCTION

Understanding the star formation history of the Universe represents an important goal of contemporary astronomy, both in theoretical modelling and from observations of the galaxy population. Traditionally, the main diagnostic used to characterise the cosmic star formation history is the volume averaged star formation rate (SFR) density (e.g. Lilly et al. 1996; Madau et al. 1996; Hopkins & Beacom 2006). This quantity encompasses the combined effect of all the physical processes that are implemented in a given theoretical model of galaxy formation. The lack of a complete theory of how these processes operate within galaxies means that these models are typically designed to be flexible, utilising simple parametrisations with adjustable model parameters. The cosmic star formation rate density, along with other global diagnostics used to assess the plausibility of a given model, is sensitive to all of these model parameters. Hence, while simply selecting a set of parameters to define a viable model is already challenging, the problem is compounded by the possibility of degeneracies between different model parameters. This has prompted the use of statistical algorithms as tools to explore and identify the allowed parameter space of contemporary galaxy formation models (Bower et al. 2010; Henriques et al. 2013; Lu et al. 2013a; Mutch et al. 2013; Ruiz et al. 2013).

⋆ E-mail: peter.mitchell@durham.ac.uk

An alternative to attempting to "solve" the entire galaxy formation problem from the top down is to try to find observational diagnostics that are sensitive to some specific physical processes but not to others. A promising area in this regard revolves around the discovery of a correlation between the star formation rate (SFR) and the stellar mass of star forming galaxies, forming a sequence of star forming galaxies (e.g. Brinchmann et al. 2004; Noeske et al. 2007a; Daddi et al. 2007; Elbaz et al. 2007). This is most convincingly demonstrated in the Sloan Digital Sky Survey (SDSS; York et al. 2000) which exhibits a clear star forming sequence with relatively small scatter and a power-law slope which is slightly below unity (e.g. Brinchmann et al. 2004; Salim et al. 2007; Peng et al. 2010; Huang et al. 2012).

The discovery of the star forming sequence in the local Universe has motivated a series of studies which try to establish whether the sequence is in place at higher redshifts (e.g. Noeske et al. 2007b). This task is challenging because of the difficulties in reliably measuring the star formation rates of galaxies. Beyond the local Universe, star formation tracers that do not require the application of uncertain dust corrections are typically available for only the most actively star forming galaxies. This makes it difficult to prove whether or not there is a clear bimodality between star forming and passive galaxies in the SFR-stellar mass plane. On the other hand, it has been demonstrated that star forming and passive galaxies can be separated on the basis of their colours over a wide range

© 2013 RAS

of redshifts (e.g. Daddi et al. 2004; Wuyts et al. 2007; Williams et al. 2009; Ilbert et al. 2010; Whitaker et al. 2011; Muzzin et al. 2013b). This technique can then be combined with stacking in order to measure the average SFR of star forming galaxies as a function of both stellar mass and redshift. However, the extent to which these convenient colour selection techniques can truly separate galaxies that reside on a tight star forming sequence from the remainder of the population remains uncertain.

The significance of the star forming sequence as a constraint on how galaxies grow in stellar mass has been discussed in a number of studies (e.g. Noeske et al. 2007b; Renzini 2009; Firmani et al. 2010; Peng et al. 2010; Leitner 2012; Heinis et al. 2014). The small scatter of the sequence implies that the star formation histories of star forming galaxies must, on average, be fairly smooth. This has been taken as evidence against a dominant contribution to the star formation history of the Universe from star formation triggered by galaxy mergers (e.g. Feulner et al. 2005; Noeske et al. 2007b; Drory & Alvarez 2008). This viewpoint is supported by studies that demonstrate that the contribution from heavily star forming objects that reside above the star forming sequence represents a negligible contribution to the number density and only a modest contribution to the star formation density of star forming galaxies (e.g. Rodighiero et al. 2011; Sargent et al. 2012).

Various studies have shown that a star forming sequence is naturally predicted both by theoretical galaxy formation models (e.g. Somerville et al. 2008; Dutton et al. 2010; Lagos et al. 2011b; Stringer et al. 2011; Ciambur et al. 2013; Lamastra et al. 2013; Lu et al. 2013b) and by hydrodynamical simulations of a cosmologically representative volume (e.g Davé 2008; Kannan et al. 2014; Torrey et al. 2014). These models have reported a slope and scatter that is generally fairly consistent with observational estimates. However, there have been a number of reported cases where it appears that the evolution in the normalisation of the sequence predicted by galaxy formation models is inconsistent with observational estimates (e.g. Daddi et al. 2007; Davé 2008; Damen et al. 2009; Santini et al. 2009; Dutton et al. 2010; Lin et al. 2012; Lamastra et al. 2013; Genel et al. 2014; González et al. 2014; Kannan et al. 2014; Torrey et al. 2014). This disagreement is often quantified by comparing model predictions with observational estimates of the specific star formation rates of galaxies of a given stellar mass as a function of redshift. This comparison can also be made for suites of hydrodynamical zoom simulations which exchange higher resolution for a loss in statistical information for the predicted galaxy formation population (Aumer et al. 2013; Hirschmann et al. 2013; Hopkins et al. 2013b; Obreja et al. 2014). These studies find that it is possible to roughly reproduce the observed specific star formation rate evolution, greatly improving over earlier simulations. However, upon closer inspection, it appears that in detail, they may suffer from a similar problem to larger simulations and semi-analytical models with reproducing the observed evolution of the star forming sequence, as noted by Aumer et al. (2013), Hopkins et al. (2013b) and Obreja et al. (2014).

It is important to be aware that below $z \approx 2$, comparisons of specific star formation rates can yield different constraints on theoretical models depending on whether or not star forming galaxies are separated from passive galaxies. In principle, if star forming galaxies are successfully separated, any disagreement in the evolution of their average specific star formation rates between models and observational data should be independent of "quenching" caused by environmental processes or AGN feedback. Hence, testing the model using the evolution in the normalisation of the star forming sequence potentially offers a significant advantage, as compared to more commonly used diagnostics such as the cosmic star formation rate density, luminosity functions and stellar mass functions. In particular, the reduced number of relevant physical processes makes the problem more tractable and offers a way to improve our understanding of galaxy formation without having to resort to exhaustive parameter space searches, where arriving at an intuitive interpretation of any results can be challenging. This is particularly pertinent if the simple parametrisations used in theoretical galaxy formation models for processes such as feedback are not suitable to capture the behaviour seen in the observed galaxy population.

Here, we use the GALFORM semi-analytic galaxy formation model along with an extensive literature compilation of observations of the star forming sequence to explore the shape of the star formation histories of galaxies within the context of a full hierarchical galaxy formation model. Our aim is to understand the origin of any discrepancies between the predicted and observed evolution in the normalisation of the star forming sequence and to demonstrate potential improvements that could be made in the modelling of the interplay between star formation, stellar feedback and the reincorporation of ejected gas.

The layout of this paper is as follows. In Section 2, we describe the relevant features of the GALFORM galaxy formation model used for this study. In Section 3, we present model predictions for the star forming sequence of galaxies and provide a comparison with a compilation of observational data extracted from the literature. In Section 4, we compare the predicted stellar mass assembly histories of star forming galaxies with the average stellar mass assembly histories inferred by integrating observations of the star forming sequence. We also explore the connection between stellar and halo mass assembly, highlighting the role of different physical processes included in the model. In Section 5, we explore modifications that can bring the model into better agreement with the data. We discuss our results and present our conclusions in Section 6 and Section 7 respectively. Appendix A provides a detailed introduction and exploration of how the stellar mass assembly histories of star forming galaxies can be inferred from observations of the star forming sequence. Appendix B discusses the impact of changing various parameters in the GALFORM model. Appendix C presents a short analysis of how well the various models presented in this paper can reproduce the evolution in the stellar mass function inferred from observations.

2 THE GALFORM GALAXY FORMATION MODEL

In this section we describe the GALFORM semi-analytic galaxy formation model, which we use to simulate the assembly of the galaxy population within the ΛCDM model of structure formation. The GALFORM model belongs to a class of galaxy formation models which connect the hierarchical assembly of dark matter haloes to galaxies by coupling merger trees generated by cosmological N-body simulations of structure formation to a series of continuity equations which control the flow of baryonic mass and metals between hot halo gas, cold disk gas and stellar components. These continuity equations are designed to encapsulate the effects of physical processes such as the inflow of gas onto galaxy disks by cooling from shock heated hydrostatic haloes. Other processes include quiescent star formation in galaxy disks, chemical enrichment of the ISM, the ejection of cold gas and metals by supernovae, the suppression of gas cooling by AGN and photoionization feedback, galaxy merging and disk instabilities which in turn can trigger

both spheroid formation and bursts of star formation. A detailed introduction to the model and the associated underlying physics can be found in Cole et al. (2000), Baugh (2006) and Benson (2010).

Rather than attempting to solve the equations of hydrodynamics to self consistently predict the full spatial distributions of stars, gas and dark matter within haloes, the equations within GALFORM can instead be solved by assuming idealised density profiles for the various components of a galaxy-halo system. For example, the hot gas and dark matter density profiles are assumed to be spherically symmetric and galaxy disks are assumed to follow an exponential surface density profile. Despite these simplifications, the lack of a complete theory of star formation and feedback processes means that the continuity equations can only be formulated and solved using a phenomenological approach.

Several variants of the GALFORM model have appeared in the literature which feature different parametrisations of the physics of galaxy formation. For this study we adopt a slightly modified version of the model presented in Lagos et al. (2012) as our fiducial model. The model used in Lagos et al. (2012) is descended from that originally presented in Bower et al. (2006) (see also Lagos et al. 2011b,a). For the fiducial model used in this study, we make a change from an older gas cooling model used in Lagos et al. (2012), which evolves according to discrete halo mass doubling events, to the continuous gas cooling model presented in Benson & Bower (2010). In the older cooling model (first presented in Cole et al. 2000), the hot gas profile is reset and the radius within which hot halo gas is allowed to cool onto a disk is reset to zero when haloes double in mass. For this analysis, we found that this simplification could lead to artificial suppression of cooling inside haloes hosting massive star forming galaxies at low redshift. Changing to a continuous cooling model removes this problem but has the side effect of slightly increasing the amount of gas available to form stars in the central galaxies of massive haloes. Therefore, in order to recover approximate agreement with the local stellar mass function of galaxies, we lower the threshold required for radio mode AGN feedback to be effective at suppressing gas cooling in our fiducial model by changing the model parameter $\alpha_{\rm cool}$ from 0.58 (as in Lagos et al. 2012) to 1.0. All of the models used in this study use merger trees extracted from the Millennium dark matter N-body simulation (Springel et al. 2005)[1]. A description of the merger tree construction can be found in Jiang et al. (2014) and Merson et al. (2013).

2.1 Star formation, supernova feedback and gas reincorporation

We now give a more detailed introduction to the treatment of several physical processes included in GALFORM that are particularly relevant to this study. Firstly, our fiducial GALFORM model uses the empirical star formation law presented in Blitz & Rosolowsky (2006), which has the form

$$\Sigma_{\rm SFR} = \nu_{\rm SF} f_{\rm mol} \Sigma_{\rm gas}, \quad (1)$$

where $\Sigma_{\rm SFR}$ is the surface density of star formation rate, $\Sigma_{\rm gas}$ is the total surface density of cold gas in the galaxy disk, $f_{\rm mol}$ is the fraction of cold hydrogen gas contained in the molecular phase and $\nu_{\rm SF}$ is the inverse of a characteristic star formation timescale. $\nu_{\rm SF}$ is constrained directly using observations of local galaxies and is set to $0.5\,{\rm Gyr}^{-1}$ for our fiducial model (Lagos et al. 2011b). $f_{\rm mol}$ is calculated using an empirical relationship which depends on the internal hydrostatic pressure of galaxy disks (Blitz & Rosolowsky 2006; Lagos et al. 2011b).

Secondly, the effects of supernova feedback are modelled by expelling cold gas from galaxy disks over each timestep as stars are formed. The outflow rate is parametrised as a function of the disk circular velocity at the half mass radius, $V_{\rm disk}$, and is given by

$$\dot{M}_{\rm ej} = \psi \left(V_{\rm disk}/V_{\rm hot}\right)^{-\alpha_{\rm hot}}, \quad (2)$$

where $V_{\rm hot}$ and $\alpha_{\rm hot}$ are numerical parameters and ψ is the star formation rate. It should be noted that these quantities refer to the outflow and star formation rates integrated over the entire galaxy disk. The outflow rate is, by convention, characterised in turn by the dimensionless mass loading factor, $\beta_{\rm ml} \equiv \dot{M}_{\rm ej}/\psi$. Unlike the parameters included in the prescription for star formation, $\alpha_{\rm hot}$ and $V_{\rm hot}$ are treated as free numerical parameters and are set in order to reproduce the observed local galaxy luminosity functions (Bower et al. 2006). For our fiducial model, $V_{\rm hot}$ is set to $485\,{\rm km\,s}^{-1}$ and $\alpha_{\rm hot}$ is set to 3.2, as in the Bower et al. (2006) and Lagos et al. (2012) models.

All of the gas that is expelled from the galaxy disk is then added to a reservoir of ejected gas which, in turn, is reincorporated at the virial temperature back into the hot gas halo at a rate given by

$$\dot{M}_{\rm hot} = \alpha_{\rm reheat} M_{\rm res}/t_{\rm dyn}, \quad (3)$$

where $\alpha_{\rm reheat}$ is a numerical parameter, $M_{\rm res}$ is the mass of gas in the reservoir and $t_{\rm dyn}$ is the dynamical timescale of the halo. For our fiducial model, $\alpha_{\rm reheat}$ is set to 1.26. Once gas is reincorporated back into the halo, it is free to cool back onto the galaxy disk. Hence, gas can be recycled many times over the lifetime of a given halo before finally being converted into stars.

2.2 Quenching processes

This cycle of gas accretion, cooling, star formation, gas expulsion and reincorporation can be disrupted in GALFORM through a number of different physical processes which we briefly outline here. The focus in this study is on actively star forming galaxies which are unaffected by these processes. Quenching mechanisms are therefore not the primary focus of our analysis as, to first order, they change which galaxies populate the star forming sequence, not the position of the sequence in the star formation rate versus stellar mass plane. Nonetheless, it is still important to recognise the conditions under which a given model galaxy will drop out of the samples of star forming galaxies which form the basis of this study.

Firstly, galaxies that form inside dark matter haloes which are accreted onto larger haloes become satellite galaxies. Satellites are assumed to lose their hot gas reservoirs to the hot gas halo of the host dark matter halo as a result of ram pressure stripping. Consequently, once a satellite uses up its cold disk gas to form stars, it will become permanently quenched. We note that the instantaneous removal of the hot gas haloes of satellites is, at best, a crude representation of the environmental processes such as ram pressure stripping. A more detailed stripping model has been explored in GALFORM (Font et al. 2008) but inclusion of this would have only

[1] Data from the Millennium and Millennium-II simulations are available on a relational database accessible from `http://galaxy-catalogue.dur.ac.uk:8080/Millennium`.

a minimal impact on the model central star forming galaxy population which will be the focus of this study.

Secondly, as the mean density of the Universe drops towards the present day, radiative cooling timescales for hot gas inside haloes grow longer. In the past, this mechanism was the key for theoretical galaxy formation models to match the observed break at the bright end of the galaxy luminosity function. However, after improved cosmological constraints favoured a higher universal baryon fraction, it was demonstrated that this mechanism could no longer fully explain the break (e.g. Benson et al. 2003). Instead, feedback associated with active galactic nuclei (AGN) is invoked as the primary mechanism responsible for quenching massive central galaxies in the current generation of galaxy formation models (e.g. De Lucia et al. 2004; Bower et al. 2006; Croton et al. 2006; Somerville et al. 2008). AGN feedback in GALFORM is implemented by assuming that cooling from the hot gas halo is completely suppressed if *a)* the halo is in a quasi-hydrostatic cooling regime and *b)* the radiative cooling luminosity of the halo is smaller than the AGN luminosity multiplied by an efficiency factor. For more details see Bower et al. (2006).

3 THE STAR FORMING SEQUENCE OF GALAXIES

In this section we first present the relationship between specific star formation rate and stellar mass predicted by our fiducial GALFORM model over a range of redshifts. We then explain how we separate star forming and passive model galaxies at different redshifts. We also present a compilation of observational data that describe how the average specific star formation rate of star forming galaxies depends on redshift and stellar mass. Finally, we compare our model predictions with the observational data.

3.1 The star forming sequence in GALFORM

Fig. 1 shows the distribution of specific star formation rate against stellar mass in our fiducial GALFORM model for a selection of redshifts. We choose to show individual galaxies as points, coloured by the logarithmic density of points at a given position in the plane. For reference, the number of galaxies shown in each redshift panel is of order 10^6. The most obvious feature that can be seen in Fig. 1 is a strong sequence of star forming galaxies that extends over several decades in stellar mass. Outliers that reside above this sequence do exist but are rare, becoming slightly more prevalent towards higher redshifts. Passive galaxies reside below the sequence, with a broad distribution of specific star formation rates at a given stellar mass.

For the remainder of this study, we choose to focus on the star forming galaxies that reside either on or above the star forming sequence. We separate passive galaxies by applying a power-law cut that evolves with redshift. The division is shown as solid blue lines in Fig. 1. The exact position and slope of the power-law cuts are fixed by hand in order to best separate the star forming sequence from the locus of passive galaxies that can be seen stretching diagonally across the plane for the most massive passive galaxies at lower redshifts. Although this is a subjective process, we find that our results are, in general, insensitive to the precise location of the cut because of the strong bimodality in the distribution. This is demonstrated by the fact that the $10^{\rm th}$ percentiles of the distribution of star forming galaxies do not reside close to our dividing line between star forming and passive galaxies in most cases. The exception to this is seen at $z = 1$ where the locus of massive passive galaxies joins onto the star forming sequence, making it difficult to objectively separate star forming from passive galaxies at $M_\star \approx 10^{11}\mathrm{M}_\odot$.

To characterise the slope and normalisation of the star forming sequence seen in Fig. 1, we adopt the convention from Karim et al. (2011) who use a power-law fit of the following functional form,

$$\psi/M_\star = c\left(\frac{M_\star}{10^{11}\mathrm{M}_\odot}\right)^{\beta_{\rm sf}}, \qquad (4)$$

where $\beta_{\rm sf}$ is the slope of the sequence and c sets the normalisation. We also define the scatter in the star forming sequence, σ, as half of the mean value over stellar mass bins of the central 68% range in the distribution of $\log_{10}(\psi/M_\star/\mathrm{Gyr}^{-1})$, calculated for each bin in stellar mass. The scatter, σ, and best fitting power-law slope, $\beta_{\rm sf}$, to the star forming sequence are labelled for each panel shown in Fig. 1. We find that the slope steepens from $\beta_{\rm sf} \approx -0.13$ at $z \leqslant 1$ up to $\beta_{\rm sf} = -0.28$ at $z = 3$. This range of slopes lies comfortably within the range of slopes that are reported by observational studies (see Appendix A3). The mean scatter, σ, does not vary strongly with redshift below $z = 3$ and is typically $\approx 0.2\,\mathrm{dex}$. The increase to $0.27\,\mathrm{dex}$ at $z = 3$ can be attributed to an increased abundance of outlying galaxies that reside above the star forming sequence at this redshift. Finally, we note that the normalisation of the star forming sequence can be seen to increase by roughly an order of magnitude over $0 < z < 3$. We explore this in greater depth in Section 3.3.

Compared to the results reported for the model from Dutton et al. (2010), the star forming sequence predicted by our fiducial model has a larger intrinsic scatter by $\Delta\sigma \approx 0.1\,\mathrm{dex}$. Dutton et al. (2010) explain that they expect their model to under-predict the scatter because their model features a simplified treatment of the mass assembly histories of dark matter haloes, neglecting various aspects of the hierarchical galaxy formation process that are included in GALFORM. On the other hand, we note that the hydrodynamical simulations presented in Torrey et al. (2014) and Obreja et al. (2014) predict a larger scatter of $\approx 0.3\,\mathrm{dex}$. This could reflect a failing of the simplified treatment of physical processes used in GALFORM when compared to a full hydrodynamical simulation. The larger scatter reported by Torrey et al. (2014) is consistent with the upper limit on the intrinsic scatter typically reported from observational studies (e.g Noeske et al. 2007b; Whitaker et al. 2012) but it is difficult to accurately assess the true uncertainty on the star formation tracers used in these studies. For the purposes of this study, the scatter in our model is small enough to be consistent with the observational upper limit and from here on, we focus instead on the slope and normalisation of the star forming sequence.

Compared to our fiducial model, the slope of the star forming sequence decreases more slowly with redshift in the Dutton et al. (2010) model, varying from $\beta_{\rm sf} = -0.04$ at $z = 0$ to -0.1 at $z = 3$. This slope is slightly shallower than predicted by our fiducial model. This could potentially be explained by the lack of any quenching or starburst processes in the Dutton et al. (2010) model. The slope of $-0.2 < \beta_{\rm sf} < -0.1$ predicted by the model presented in Lamastra et al. (2013) is consistent with our fiducial model although this somewhat unsurprising given the many similarities between the two models. On the other hand, the hydrodynamical simulations presented in Torrey et al. (2014) report a slope of $-0.05 < \beta_{\rm sf} < 0.0$ which is more similar to Dutton et al. (2010). Obreja et al. (2014) also find a slope consistent with $\beta_{\rm sf} = 0$.

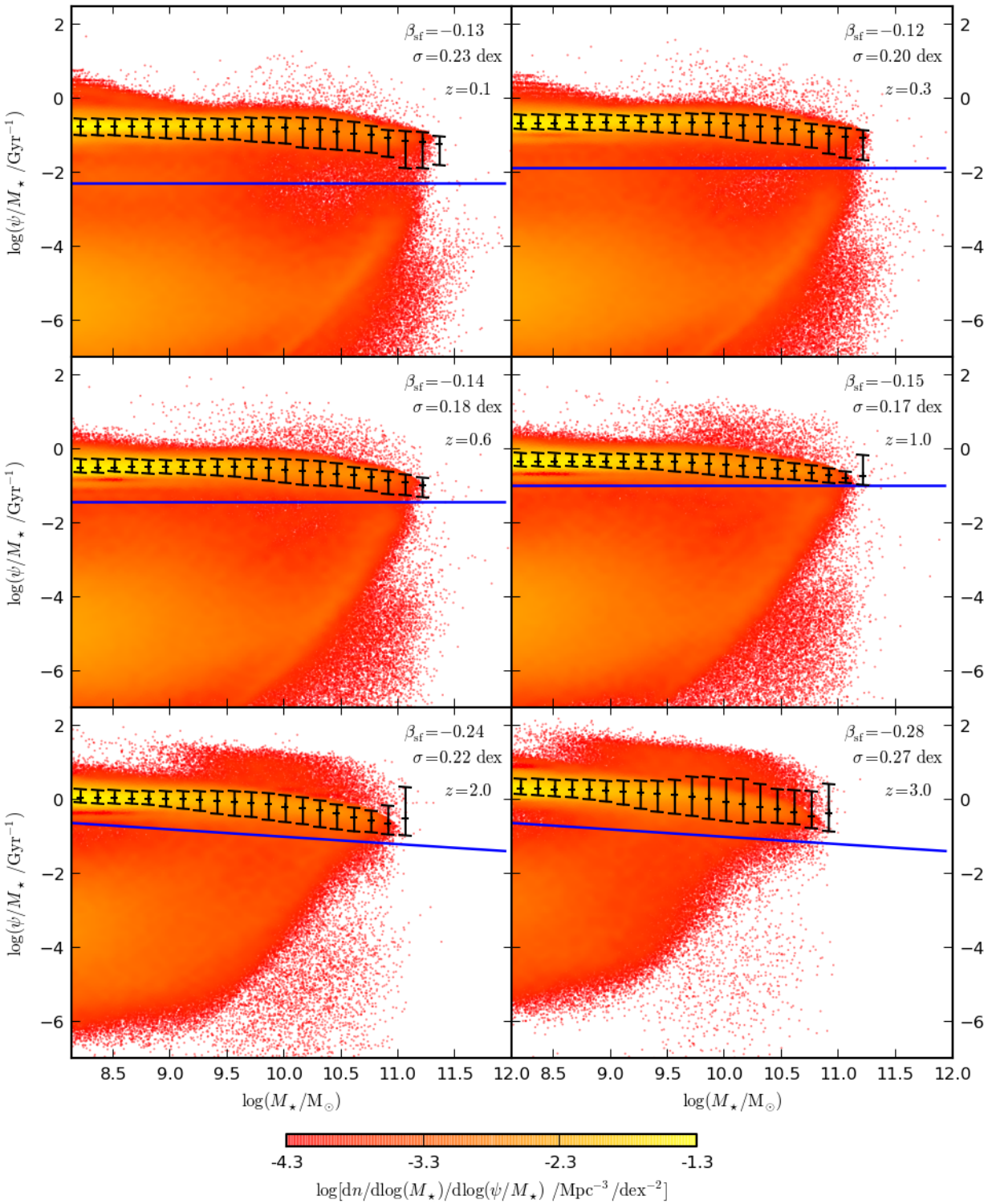

Figure 1. Specific star formation rate plotted as a function of stellar mass for all galaxies from our fiducial GALFORM model. Each panel corresponds to a different redshift as labelled. The coloured points represent individual model galaxies and the point colours are scaled logarithmically with the local number density of galaxies in each panel, from red at low density to yellow at high density. The corresponding number densities are indicated by the colour bar at the bottom of the figure. The blue lines show our cut between star forming and passive galaxies for each redshift. The black points and corresponding error bars show the median, $10^{\rm th}$ and $90^{\rm th}$ percentiles of the distribution in the specific star formation rates of star forming galaxies, binned as a function of stellar mass. $\beta_{\rm sf}$ is the slope of a power-law fit to the medians of the distribution for star forming galaxies. σ quantifies the average scatter and is defined as half of the mean central 68% range of the distribution for star forming galaxies.

Source	Redshift	Selection	SF cut	Tracer
Noeske et al. (2007a)	0.2-1.1	K	blue colour/24μm detection	24μm+UV/Em Lines
SDSS DR7	0.08	r	sSFR-$M_\star$ distribution	H_α
Pannella et al. (2009)	1.5-2.5	BzK	sBzK	Radio
Oliver et al. (2010)	0-2	Optical	template fitting	$70/160\mu$m
Magdis et al. (2010)	3	LBG	blue colour	UV (corrected)
Peng et al. (2010)	0-1	Optical	blue colour	SED fitting
Rodighiero et al. (2010)	0-2.5	4.5μm	blue colour/24μm detection	FIR
Karim et al. (2011)	0.2-3	3.6μm	blue colour	Radio
Huang et al. (2012)	0	HI / r	HI detection/blue colour	SED fitting
Lin et al. (2012)	1.8-2.2	BzK	sBzK	UV (corrected)
Reddy et al. (2012)	1.4-3.7	LBG	blue colour	24μm+UV
Whitaker et al. (2012)	0-2.5	K	(U-V/V-J) cut	24μm+UV
Bauer et al. (2013)	0.05-0.32	r	H_α flux/EW	H_α
Stark et al. (2013)	4-7	LBG	blue colour	UV (corrected)
Wang et al. (2013)	0.2-2	K	SFR-$M_\star$ distribution	SED fitting / FIR
González et al. (2014)	4-6	LBG	blue colour	SED fitting

Table 1. List of the sources of the observed average specific star formation rates of star forming galaxies, $\langle\psi/M_\star\rangle(M_\star, z)$, which we extract from the literature. We list the source, redshift range or median redshift, galaxy selection technique, the subsequent star forming galaxy selection technique, and the tracer used to estimate the instantaneous star formation rate. For LBG-selected samples, it should be noted that the initial galaxy selection technique is strongly biased towards blue star forming galaxies, so typically no additional cut to separate star forming galaxies is performed. SDSS DR7 data are taken from the public webpage `http://www.mpa-garching.mpg.de/SDSS/DR7/`, which corresponds to an update of the Brinchmann et al. (2004) analysis. For Karim et al. (2011), we use both the star forming galaxy sample presented in their Table 3 as well as the "active population" which is shown in their Figure 13 (which uses a bluer colour cut). The code and observational data used for this compilation are available at `http://www.astro.dur.ac.uk/~d72fqv/average_sSFR_SFGs/`.

3.2 The star forming sequence inferred from observations

For this study, we have compiled a set of observational data on the star forming sequence for the purposes of providing a comparison with model predictions. Specifically, we have compiled the average specific star formation rate of star forming galaxies for bins of stellar mass and redshift. Both mean and median star formation rates have been used to quantify the average in the literature and we include both quantities in the compilation. The list of sources used in the compilation is presented in Table 1. We include information on the redshift range covered, the initial selection technique, the technique to separate star forming galaxies and the star formation rate tracer used. We only include observational data sets that have either made an attempt to separate star forming galaxies from passive galaxies or have a selection function which intrinsically selects only actively star forming objects. Where necessary, we convert stellar masses quoted that assume a Salpeter IMF by $\Delta\log(M_\star/\mathrm{M}_\odot) = -0.24\,\mathrm{dex}$ in order to be consistent with a Chabrier IMF (Ilbert et al. 2010; Mitchell et al. 2013), which in turn is very similar to the Kennicutt IMF that is assumed in our model. We do not attempt to correct specific star formation rates for IMF variations as we expect both the stellar mass and star formation rate corrections to approximately cancel in most cases.

It is very important to be aware that the average star formation rate, particularly for large stellar masses at low redshift, will depend strongly on the method used to separate star forming from passive galaxies. In general, it is not possible in practice to simply make the separation based on identifying the star forming sequence in the star formation rate versus stellar mass plane. This is only really possible in the local Universe with surveys such as the SDSS. Instead, star forming galaxies are often separated using colour selection criteria (e.g. Daddi et al. 2004; Ilbert et al. 2010). These issues are particularly pertinent for studies that employ stacking techniques, where it is impossible to ascertain whether a star forming sequence is really present in the data (Oliver et al. 2010; Rodighiero et al. 2010; Elbaz et al. 2011; Karim et al. 2011).

3.3 Comparing the star forming sequence from GALFORM with observational data

Fig. 2 shows the average specific star formation rates of star forming galaxies as a function of stellar mass for a selection of redshifts. Observational data from the compilation presented in Table 1 are shown in grey and can be compared to the mean and median relations predicted by the our fiducial model. It should be noted that the error bars on the observational data points show only a lower limit on the statistical uncertainty on each data point. These error bars are only shown for the studies where an estimate of this lower limit could be obtained. The error bars do not represent the dispersion in the underlying distribution. We attempt to estimate a more realistic uncertainty on the average specific star formation rate by measuring the average central 68% range for measurements in all stellar mass bins containing more than two data points. We find that the uncertainty on the specific star formation rate estimated in this way is $0.20\,\mathrm{dex}$. The pink shaded regions shown in Fig. 2 then enclose the set of best fitting power laws to the data within a 1σ range, assuming $0.2\,\mathrm{dex}$ errors in each mass bin.

Given the large systematic uncertainties that are thought to affect stellar mass and SFR estimates and that each data set uses a different method to select star forming galaxies, it is reassuring that the observational data are fairly self consistent in normalisation within each respective redshift panel. There are some outlying data sets however. In general, the observations seem consistent with a star forming sequence where the average specific star formation rate is modestly anti-correlated with stellar mass. We note however that there are significant variations in the slope seen between different redshift panels. The best fitting power-law slopes at each redshift vary from $\beta_{\mathrm{sf}} \approx -0.4$ at $z = 0$ to $\beta_{\mathrm{sf}} \approx 0.1$ at $z = 3$. Whether or not this variation is driven by an intrinsic shift in the

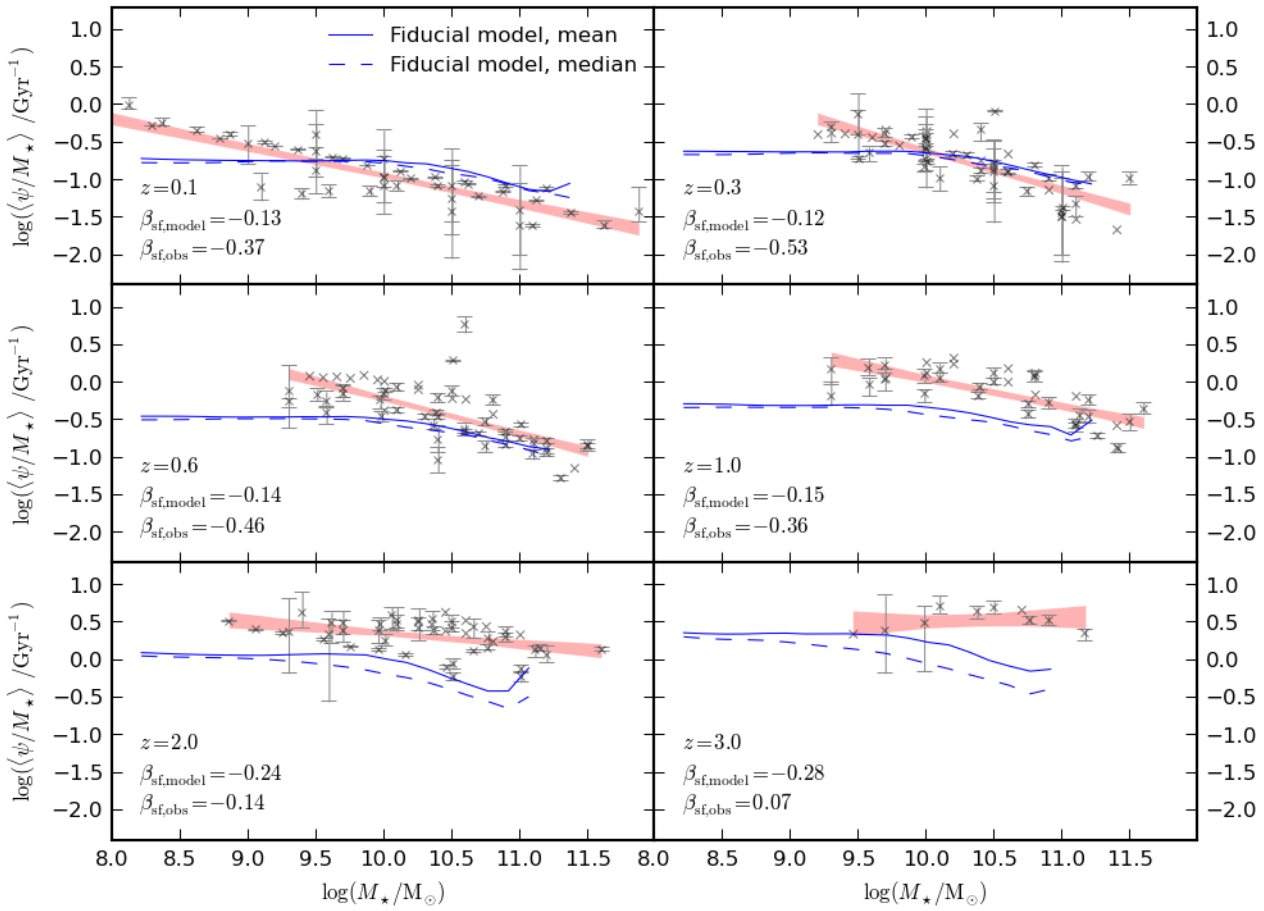

Figure 2. The average specific star formation rate of star forming galaxies plotted as a function of stellar mass. Each panel corresponds to a different redshift as labelled. Blue solid and dashed lines show predictions from our fiducial GALFORM model for the mean and median specific star formation rates respectively. Grey points show observational estimates of either the mean or median average specific star formation rate of star forming galaxies. A list of the sources of these observational data points is presented in Table 1. When shown, the corresponding error bars show a lower limit on the statistical uncertainty on the average for each data point. The shaded region shows the 1σ range of power-law fits to the observational data, using a fixed error on the data points of 0.20 dex. $\beta_{\rm sf,model}$ is the best fitting power-law slope to the medians of the distribution predicted by our fiducial model. $\beta_{\rm sf,obs}$ is the best fitting power-law slope to the observational data presented in each panel.

slope of a star forming sequence of galaxies is extremely unclear. We explore this issue in more detail in Appendix A3.

Comparison of the observed slope with predictions from our fiducial model indicates that the model has a slope which is too shallow at low redshift and too steep at high redshift. In addition, compared to the data, the slope variation with redshift acts in the opposite direction in the model, such that the high redshift slope is steeper than the local relation. However, it is difficult to be confident whether this truly reflects a flaw in the model or can be explained as a result of selection effects. To answer this question satisfactorily would require a self-consistent comparison between the model and the data in terms of selection. However, this task is made challenging because of the difficulty in predicting accurate colour distributions for galaxies from hierarchical galaxy formation models. Historically, various GALFORM models have struggled to reproduce the observed colour distributions of galaxies, making it difficult to reproduce observational colour cuts in detail (e.g. Guo et al. 2013).

Although it is difficult to draw strong conclusions from comparing the slopes of the observed and predicted distributions, it is apparent that the normalisation of the star forming sequence evolves more rapidly in the observational data than in the model. This problem is best viewed by plotting the evolution of the average specific star formation rate of star forming galaxies as a function of lookback time for selected stellar mass bins, which we show in Fig. 3. In general, we find that the observational data are consistent with exponential evolution in $\langle\psi/M_\star\rangle$ with lookback time. The best fit to the observational data in each panel gives $\langle\psi/M_\star\rangle \propto e^{a\,t_{\rm lb}}$ where a is found to vary between 0.29 and 0.43. The variation in a is such that the average specific star formation rate drops more rapidly with time in the highest mass bins shown. Although there is some scatter at a given redshift, the data within each mass bin appear to be mostly self consistent in normalisation at a given redshift. Repeating the same process as for Fig. 2, we estimate the uncertainty on the average specific star formation rates and again find that the uncertainty is approximately 0.20 dex.

In contrast to the trend that emerges from the observational compilation, our fiducial model (blue lines) predicts slower evolu-

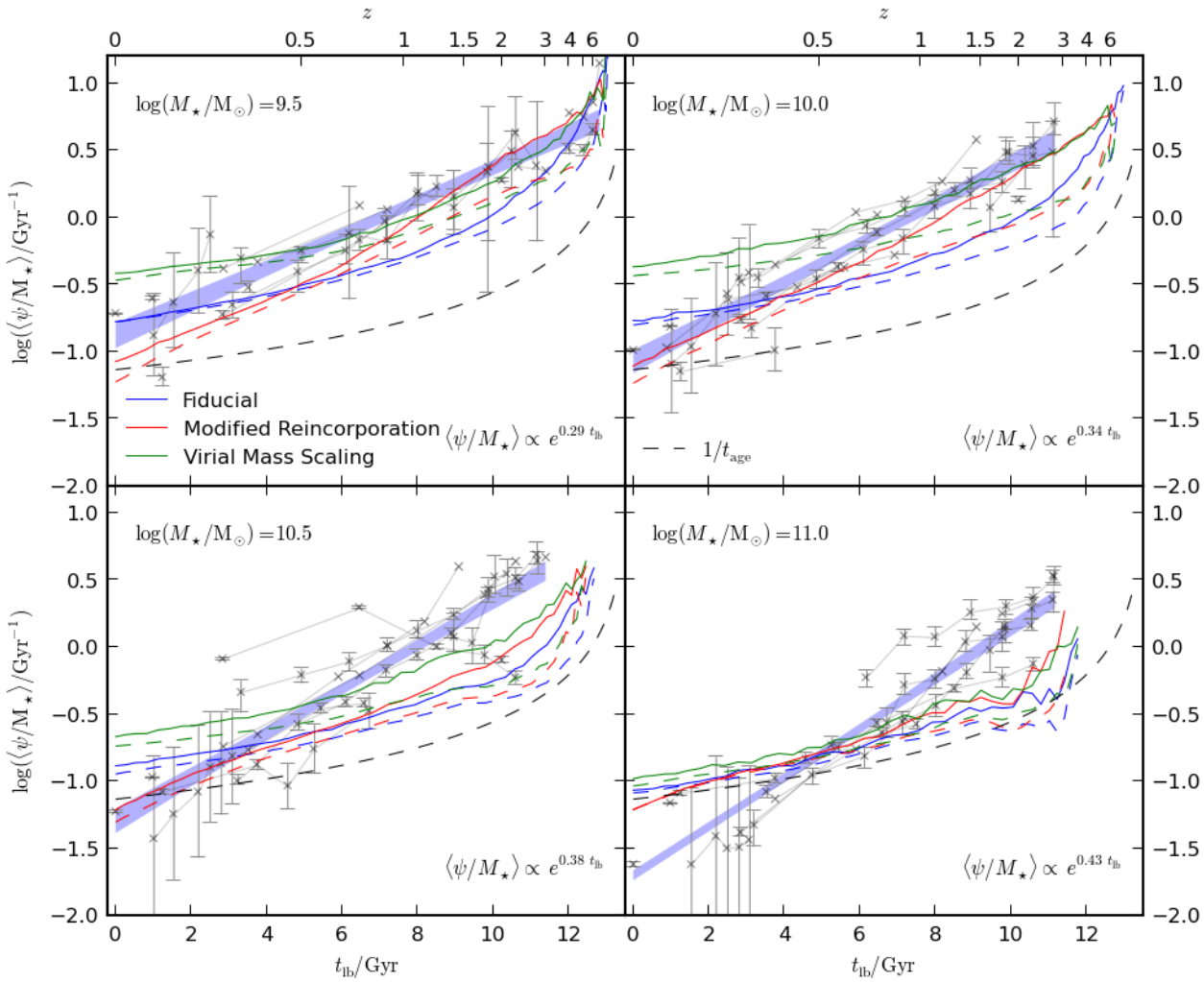

Figure 3. The average specific star formation rate of star forming galaxies plotted as a function of lookback time. Each panel corresponds to a different stellar mass bin as labelled. Blue solid and dashed lines show predictions from our fiducial GALFORM model for the mean and median specific star formation rates respectively. Red lines show the same information but for the modified reincorporation model. Green lines show the same information but for a model using the virial mass scaling for the reincorporation timescale proposed by Henriques et al. (2013). Dashed black lines show the inverse of the age of the universe as a function of lookback time. Grey points show observational estimates of either the mean or median average specific star formation rate of star forming galaxies. A list of the sources of these observational data points is presented in Table 1. When shown, the corresponding error bars show a lower limit on the statistical uncertainty on the average for each data point. Grey points taken from a single observational study are connected by grey lines. The blue shaded region shows the 1σ range of exponential fits to the observational data, assuming a fixed error on the data points of 0.20 dex. This shaded region is consistent with, but not identical to, the pink shaded region shown in Fig. 2. The best fit to the evolution in the observational data is given in each panel.

tion than the data (until higher redshifts, where the evolution in the model becomes steeper than an extrapolation of the trend seen in the data). This behaviour has been seen for various published models in the literature (e.g. Davé 2008; Damen et al. 2009; Dutton et al. 2010; González et al. 2014; Torrey et al. 2014) and the origin of the discrepancy is the subject of the remainder of this paper. Finally, at this stage we note that the evolution in the fiducial GALFORM model scales very closely with the inverse of the age of the universe at a given time, $t_{\rm age}$. We return to this point in Section 4.2.

4 THE STELLAR MASS ASSEMBLY OF STAR FORMING GALAXIES

It is clear from Fig. 3 that the specific star formation rates of galaxies at a fixed stellar mass evolve more slowly with redshift in our fiducial GALFORM model than is implied by the observational data. However, it should be noted that the galaxy population which is probed at each redshift for a given stellar mass bin will not be the same; star forming galaxies grow in stellar mass before becoming quenched and consequently dropping out of the star forming samples which we consider. This complicates the interpretation of Fig. 3 with regard to understanding the physical origin of any flaws in the model.

It is therefore worthwhile to search for a another way to characterise the evolution of star forming galaxies which traces only a

single population across cosmic time. One way to achieve this is to try to infer the stellar mass assembly histories of star forming galaxies by tracing how they grow in stellar mass as they evolve along a star forming sequence. This technique has already appeared in various guises in the literature (e.g. Drory & Alvarez 2008; Renzini 2009; Leitner & Kravtsov 2011; Leitner 2012; Heinis et al. 2014). From here on in, we adopt the terminology of Leitner (2012) and refer to this technique as Main Sequence Integration (MSI).

In this section, we explore the origin of the discrepancy between the predicted and observed evolution in the specific star formation rates of star forming galaxies shown in Fig. 3 We start by making use of the MSI technique to compare the predicted and observationally inferred stellar mass assembly histories of galaxies that are still star forming at $z = 0$. We then go on to discuss why the predicted stellar mass assembly histories have a particular form, connecting the halo assembly process with the way stellar feedback is implemented in our model.

An introduction to the MSI technique is presented in Appendix A1. An exploration of how well MSI can recover the predicted stellar mass assembly histories calculated in our model can be found in Appendix A2. Details of the observational compilation of measurements of the star forming sequence which we use for this study can be found in Appendix A3.

4.1 Comparing the inferred stellar mass assembly histories of star forming galaxies with model predictions

In Fig. 4, we compare the predicted average stellar mass assembly histories of central galaxies that are still star forming at $z = 0$ from our fiducial GALFORM model with the results of applying MSI to the observational compilation presented in Appendix A3. To facilitate a comparison with the average stellar mass assembly histories obtained using the MSI technique for a given starting mass, model galaxies are binned by their stellar mass at $z = 0$. By default in this study, stellar mass assembly histories are obtained by tracing back the main stellar progenitor of each $z = 0$ central star forming galaxy. We define the main stellar progenitor as the most massive stellar progenitor traced between each consecutive pair of output times. The impact of this choice (as compared to summing over all possible progenitors) is discussed in Appendix A2. We have chosen to plot $\langle \dot{M}_\star / M_\star(t_0) \rangle$ in order to eliminate dispersion associated with the finite width of the stellar mass bins which we use ($\Delta \log(M_\star \, / \mathrm{M}_\odot) = 0.5\,\mathrm{dex}$). The remaining dispersion therefore reflects the intrinsic scatter in our model in the shape of stellar mass assembly histories of galaxies that are central and star forming at $z = 0$. The choice to include only galaxies that are central at $z = 0$ is made in order to minimise the impact of any environmental effects. When comparing to mass assembly histories inferred from observations (which include a combination of satellite and central galaxies), the exclusion of satellite galaxies is justified by observational results that indicate that the form of the star forming sequence is independent of environment (e.g. Peng et al. 2010).

Quantitatively, the model predicts stellar mass assembly rates that are broadly consistent to within factors of 2 compared to the data. However, despite the weak constraints provided by MSI in some cases, there is a clear qualitative disagreement between the model and the data regarding the shape of the stellar mass assembly histories predicted by GALFORM. In the model, the rate of star formation rises rapidly at early times before slowing down to a gradual rise or to a constant level of activity at later times. The observational data instead favours a scenario where star formation activity builds towards a peak at an intermediate time before dropping significantly towards $z = 0$. This disagreement is consistent with the trend seen in Fig. 3 where the specific star formation rates of galaxies in the model are too low compared to the data at intermediate times before rapidly rising towards high redshift.

At this stage, it should be noted that our fiducial model is only one specific realisation of GALFORM with regard to the various model parameters that can be changed. While these parameters are constrained by requiring that the model matches local global diagnostics of the galaxy population, it is important to understand whether the disagreement between predictions and data seen in Fig. 3 and Fig. 4 is specific to the combination of parameters used in our fiducial model. An analysis of this issue if presented in Appendix B. To summarise, we find that for a given stellar mass at $z = 0$, the shapes of the average stellar mass assembly histories of central star forming galaxies in GALFORM are almost entirely invariant when changing model parameters relating to star formation, feedback and gas reincorporation. As a consequence, the disagreements seen in Fig. 3 and Fig. 4 do indeed seem to be generic for any model that uses the same parametrisations to represent these physical processes. This also helps to explain why similar models find a similar disagreement in other studies.

As well as stellar mass assembly histories, we also show in Fig. 4 the corresponding average dark matter halo mass assembly histories of central galaxies from our fiducial GALFORM model that are star forming at $z = 0$. We choose to define the dark matter halo mass assembly rate, $\dot{M}_\mathrm{H}$, by tracing backwards the host halo of the main stellar progenitor (see Appendix A2). This definition is useful for making comparisons with the stellar mass assembly process. However, it should be noted that in some cases this definition could deviate from the standard definition of halo mass assembly histories where instead the main halo progenitor is traced backwards (e.g Fakhouri et al. 2010). To quantify the average halo mass assembly rate, we take the mean of the distribution at each lookback time. This choice is made because the individual halo assembly histories are very stochastic with respect to our temporal resolution (which is determined by the number of available outputs from the Millennium simulation). As a consequence, we find that only the mean halo mass assembly history integrates to the correct average halo mass at $z = 0$ while the median does not. Incidentally, this stochasticity is why even the average halo mass assembly histories shown in Fig. 4 get visibly noisy towards late times due to a drop in the average rate of significant accretion events.

From Fig. 4, we can begin to understand why there is a disagreement in the stellar mass assembly process between our fiducial GALFORM model and the trends implied by the data. In the model, despite the enormous variation in the efficiency of star formation relative to gas accretion between haloes of different mass at $z = 0$, stellar mass assembly broadly tracks the halo assembly process. Stars start to form as soon as their host haloes accrete an appreciable fraction of their final mass and this continues all the way to the present day. Differences between the stellar and halo assembly histories do exist however. For example, the stellar mass assembly histories do not show the peak at $t_\mathrm{lb} \approx 12\,\mathrm{Gyr}$ which is fairly prominent for the haloes. Also, the halo accretion rates fall slowly towards late times after this peak, whereas most star forming galaxies form stellar mass at either a constant or slightly increasing rate over their lifetimes. However, the decline in the halo mass accretion rates is generally not as steep as the rate of decline in star formation rates inferred from the observational data. This can be seen more clearly in Fig. 5 where we show the ratio of the rates of mean stellar mass assembly to halo mass assembly.

In order to broadly reproduce the observed $z = 0$ stellar mass

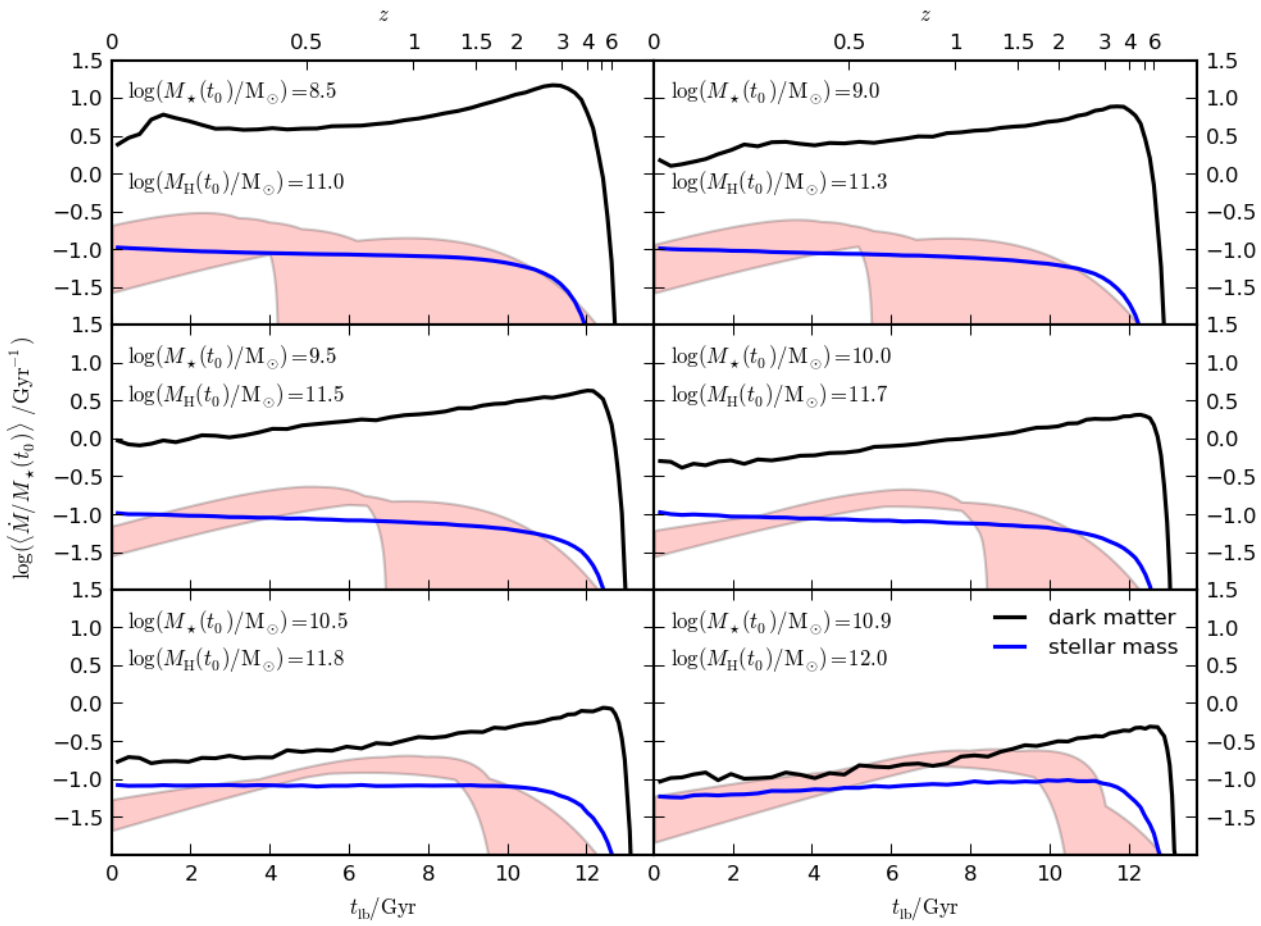

Figure 4. The mean mass assembly histories of galaxies that are central and star forming at $z = 0$, plotted as a function of lookback time. Blue lines show predictions for the mean stellar mass assembly histories for the main stellar progenitors of central galaxies, taken directly from our fiducial GALFORM model. Black lines show the corresponding dark matter halo mass assembly histories of the progenitor haloes that host the main stellar progenitors of central galaxies at $z = 0$. These curves are rescaled by $f_{\rm b} \equiv \Omega_{\rm b}/\Omega_{\rm M}$ to show the baryonic accretion rate onto these haloes. Model galaxies are binned by their stellar mass at $z = 0$, with each panel corresponding to a different mass bin. The median $z = 0$ stellar mass in each bin is labelled in each panel. The corresponding median $z = 0$ dark matter halo mass in each stellar mass bin is also labelled. The filled pink region shows the range of stellar mass assembly histories that are inferred by applying the MSI technique to observational data from the literature.

or luminosity functions, it is necessary that a given galaxy population model, on average, places galaxies of a given stellar mass inside haloes of the mass corresponding approximately to the correct abundance. Given that our fiducial GALFORM model roughly reproduces the local stellar mass function, the halo assembly histories shown in Fig. 4 should therefore correspond roughly to the true halo formation histories of real galaxies, for the case of a ΛCDM universe. Adopting this as a working assumption, we also show in Fig. 5 the efficiency of star formation inferred from observations using MSI if we use the relationship between stellar mass and halo mass at $z = 0$ for star forming galaxies in our model. This extra step allows us to infer how efficiently haloes that host star forming galaxies at $z = 0$ convert accreted baryons into stars. It can be seen that in the model, the efficiency of star formation relative to halo gas accretion rises monotonically from early times to the present day, whereas the data, in general, favours a scenario where this efficiency peaks at some intermediate time for the higher stellar mass bins.

In Appendix A3, we discuss how, depending on the slope of the observed star forming sequence, $\beta_{\rm sf}$, the inferred stellar mass assembly of galaxies that are still star forming at $z = 0$ can show a downsizing trend, such that the lower mass star forming galaxies start forming stars later with respect to massive star forming galaxies. Fig. 4 shows that any possible downsizing trend suggested by the data is, at best, only weakly reproduced by the model. The different stellar mass assembly histories that we infer from the observational data agree best with our model for the $\beta_{\rm sf} = 0.0$ or -0.1 cases shown in Fig. A5. The assembly histories derived from these bins show the weakest downsizing trend (no downsizing for $\beta_{\rm sf} = 0.0$) and form a greater fraction of stars at early times. It should be noted that the better agreement with the model for these curves is not surprising given that the slope of the star forming sequence in the fiducial GALFORM model is $\beta_{\rm sf} \approx -0.15$. For the opposite extreme case in the data where $\beta_{\rm sf} \approx -0.5$, the model predictions are in dramatic disagreement with the trends implied by the data for low mass galaxies.

Another consequence of a strong downsizing trend is that the stellar mass assembly process is significantly delayed relative to

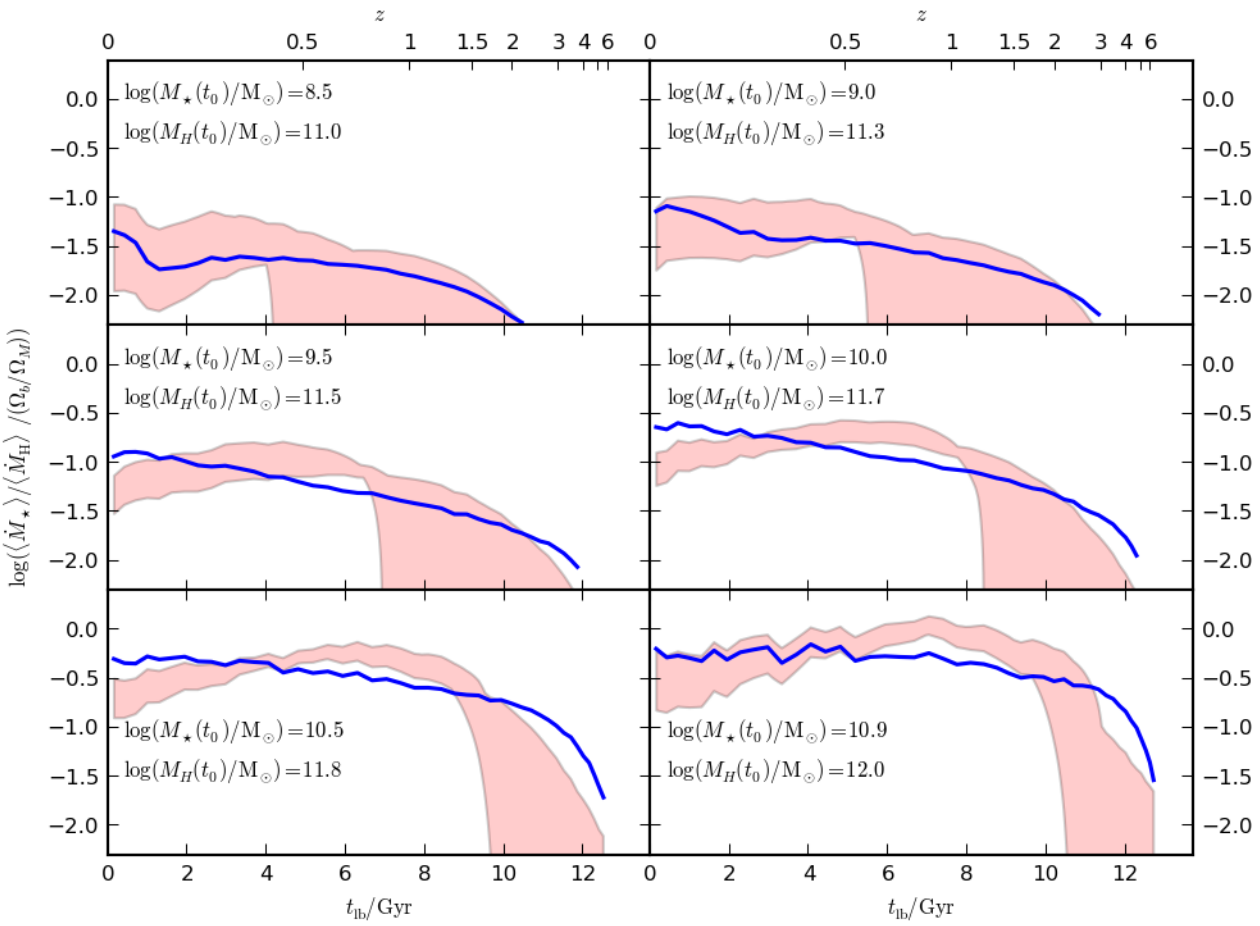

Figure 5. The ratio of mean stellar mass assembly rate to mean baryonic halo mass assembly rate for galaxies that are star forming at $z = 0$, plotted as a function of lookback time. Blue lines show predictions from our fiducial GALFORM model for this ratio for galaxies that are central at $z = 0$. Model galaxies are binned according to their $z = 0$ stellar mass with each panel corresponding to a different mass bin. The median $z = 0$ stellar mass in each bin is labelled in each panel. The corresponding median $z = 0$ dark matter halo mass of each stellar mass bin is also labelled. The filled pink regions show the range in the ratio of galaxy to halo mass assembly rates inferred from observational data. This is obtained using a combination of stellar mass assembly histories inferred from observational data using the MSI technique and average halo mass assembly histories from GALFORM. This assumes that the true ratio between stellar mass and halo mass at $z = 0$ is the same as in our fiducial GALFORM model.

the halo assembly process for low mass systems. Fig. 4 shows that the shape of the mean halo mass assembly histories is only a very weak function of the final halo mass. Therefore, any possible downsizing trend that exists purely in the star forming population would have to be caused by a physical process which is separate from the growth of the hosting dark matter haloes. For the case where $\beta_{\rm sf} \approx -0.4$, such a process would result in the existence of a population of dark haloes that have not formed any appreciable amount of stars at intermediate redshifts of $1 < z < 2$. We note that the star formation histories presented in Leitner (2012), derived by applying MSI to data from Karim et al. (2011) with $\beta_{\rm sf} = -0.35$ and from Oliver et al. (2010), would also have this consequence. Reproducing this behaviour in models or simulations would require much stronger feedback (or the inclusion of another physical mechanism with the same effect) at early times than is typically assumed for galaxies that reside within the progenitors of haloes of mass $11 < \log(M_{\rm H}(t_0)/{\rm M}_\odot) < 12$.

4.2 Explaining the form of stellar mass assembly histories in GALFORM

In Section 4.1, we show that the stellar mass assembly process in our fiducial GALFORM model broadly traces the halo mass assembly process. The closeness in this predicted co-evolution appears to be in qualitative disagreement with trends inferred from the star formation rates of galaxies inferred from observational data. This leads to the slower evolution in the predicted average specific star formation rates of star forming galaxies compared to the observational data seen in Fig. 3. Fig. 3 also demonstrates that this evolution in the model closely traces the inverse of the age of the universe, $t_{\rm age}$, such that $\psi/M_\star \propto 1/t_{\rm age}$. We now consider why the model behaves in this way.

i) Cooling timescale: For the star forming galaxy population which we consider in this study, we expect the radiative cooling timescales for shock heated halo gas to cool onto galaxy disks to be short compared to the age of the Universe at a given epoch. In the top panel of Fig. 6, we see that this is indeed the case if we trace backwards the main stellar progenitors of galaxies that are central

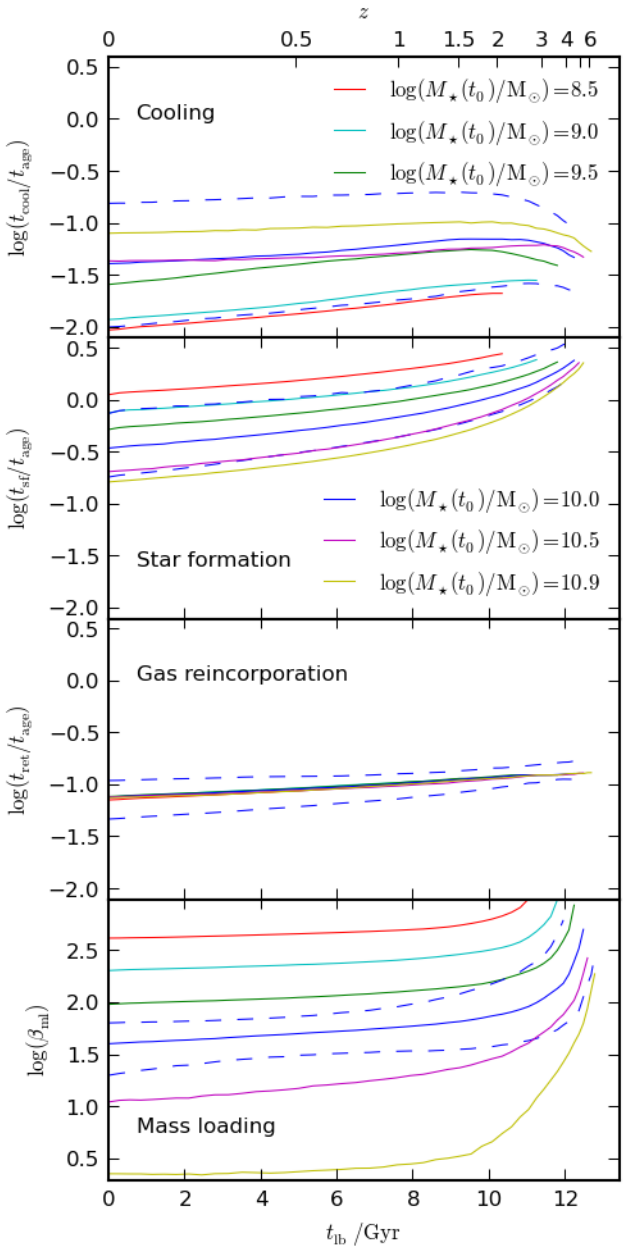

Figure 6. The ratio of average characteristic timescales of model galaxies which are central and star forming at $z = 0$ to the age of the universe, $t_{\rm age}$, plotted as a function of lookback time. Model galaxies are binned according to their $z = 0$ stellar mass with each solid coloured line showing the median of the distribution for a different bin. The blue dashed lines show the $10^{\rm th}$ and $90^{\rm th}$ percentiles for the $\log(M_\star(t_0)/{\rm M}_\odot) = 10$ bin. The top three panels each correspond to a different timescale. The bottom panel instead shows the efficiency with which gas is ejected from galaxy disks. *Top:* The characteristic gas cooling timescale, $t_{\rm cool}$, for hot halo gas to cool onto a galaxy disk. *Second:* The characteristic star formation timescale, $t_{\rm sf}$, for disk gas to be converted to stars in the absence of feedback. *Third:* The characteristic gas reincorporation timescale, $t_{\rm ret}$, for gas ejected by feedback to be reincorporated back into the hot gas halo. *Bottom:* The mass loading factor of outflows, $\beta_{\rm ml}$.

and star forming at $z = 0$, following the methodology introduced in Section 4.1. We define the characteristic cooling timescale, $t_{\rm cool}$, as the time for gas with the mean density within the virial radius to cool. Given that this timescale is short, the only three remaining physical processes in the model which are relevant for the star forming galaxy population considered here are star formation, outflows triggered by SNe feedback and the subsequent reincorporation of ejected gas back into the hot halo gas component.

ii) Star formation timescale: The efficiency of star formation can be characterised by the timescale required to consume cold disk gas in the absence of feedback. This is given by $t_{\rm sf} \equiv M_{\rm cold}(t)/\psi(t)$. We show the average evolution in this quantity for the star forming population in the second panel of Fig. 6, relative to the age of the universe at a given epoch. It can be seen that this timescale is typically comparable to the age of the universe, although there is an order of magnitude variation depending on the time and final stellar mass of the galaxies being considered. The consequence of the balance between the star formation timescale and the age of the Universe is that cooling gas can be effectively converted into stars in a quasi-steady state. In practice, the true gas depletion timescale will be significantly shorter than $t_{\rm sf}$ in the model when the mass loading factor of outflows, $\beta_{\rm ml}$, rises above unity, which is typically the case for the galaxies considered here.

iii) Mass loading factor: In our model, the efficiency of SNe feedback in ejecting cold gas from galaxies is characterised by the mass loading factor, $\beta_{\rm ml}$. The average evolution in $\beta_{\rm ml}$ is shown in the bottom panel of Fig. 6. As described in Section 2.1, $\beta_{\rm ml}$ in our fiducial GALFORM model scales $\propto V_{\rm disk}^{-3.2}$, where $V_{\rm disk}$ is the circular velocity of the galaxy disk at the half mass radius. The evolution in this quantity over the lifetime of the star forming galaxies which we consider here is very modest. In general, $V_{\rm disk}$ rises at early times before becoming almost constant at intermediate to late times. This lack of evolution in $V_{\rm disk}$ is primarily driven by the corresponding lack of evolution in the circular velocity of the host haloes at the virial radius, $V_{\rm vir}$. The strong scaling of $\beta_{\rm ml}$ with $V_{\rm disk}$ means that there is a stronger evolution in the efficiency of feedback with lookback time, particularly for massive galaxies at early times where $\beta_{\rm ml}$ grows significantly above unity. The increased feedback efficiency at early times explains why the galaxy stellar mass assembly histories do not share the peak at $t_{\rm lb} \approx 12$ Gyr seen for the halo mass assembly histories shown in Fig. 4. At late times, $\beta_{\rm ml}$ becomes approximately constant in time for all galaxies, which will result in a fixed modulation of the efficiency in converting accreted gas into stars.

iv) Reincorporation timescale: It is also important to consider how efficiently gas that is ejected by feedback is able to return back into the hot gas halo. As described in Section 2.1, ejected gas is placed into a reservoir of mass $M_{\rm res}$. This gas then returns to the halo on a characteristic timescale given by $t_{\rm ret}(t) \equiv M_{\rm res}/\dot{M}_{\rm ret}$ (Bower et al. 2006). In GALFORM, this quantity scales $\propto t_{\rm dyn}^{-1}$ where $t_{\rm dyn}$ is the halo dynamical time (see Eqn. 3). We characterise the efficiency of gas reincorporation by $t_{\rm ret}/t_{\rm age}$. The average evolution in this reincorporation timescale for model galaxies that are central and star forming at $z = 0$ is shown in the third panel of Fig. 6. This shows that the timescale for reincorporation is close to an order of magnitude shorter than the age of the universe at all times. The timescale is also almost completely independent of the final stellar or halo mass. This is because the halo dynamical time, to first order, depends only on the current mean density of the universe. As the mean density of the universe falls with time, so does the timescale for reincorporation.

By combining the picture that is presented in Fig. 6 with sim-

ple arguments, we now proceed to demonstrate analytically the origin of the behaviour seen in Fig. 3 for the predicted evolution of the specific star formation rates of star forming galaxies. Firstly, we can relate the mean density of a halo, $\bar{\rho}_{\rm H}$ to the circular velocity at the virial radius, $V_{\rm vir}$, and the virial radius, $R_{\rm vir}$, through

$$\bar{\rho}_{\rm H} = \frac{3}{4\pi}\frac{M_{\rm H}}{R_{\rm vir}^3} = \frac{3}{4\pi G^3}\frac{V_{\rm vir}^6}{M_{\rm H}^2}. \quad (5)$$

This can be rearranged into

$$M_{\rm H} \propto \bar{\rho}_{\rm H}^{-0.5} V_{\rm vir}^3. \quad (6)$$

The average density of a halo can be related to the mean density of the universe, $\bar{\rho}$, by

$$\bar{\rho}_{\rm H} = \Delta_{\rm v}\bar{\rho}, \quad (7)$$

where $\Delta_{\rm v}$ is the mean overdensity given by the spherical collapse model (Gunn & Gott 1972). For the simplified case of an $\Omega_{\rm M} = 1$ universe, $\Delta_{\rm v} = 18\pi^2$ and $\bar{\rho} \propto 1/t_{\rm age}^2$. In this case, we can write

$$M_{\rm H} \propto t_{\rm age}\, V_{\rm vir}^3. \quad (8)$$

As discussed earlier, evolution in $V_{\rm vir}$ over the lifetime of a given galaxy is weak, particularly at intermediate to late times. We can therefore make the approximation that $V_{\rm vir}$ is constant with time, yielding

$$\dot{M}_{\rm H} \propto V_{\rm vir}^3. \quad (9)$$

If we temporarily ignore gas reincorporation and assume that the star formation, freefall and cooling timescales of a halo are all short, then balancing the rate of accretion of gas to star formation and gas ejection gives

$$f_{\rm b}\dot{M}_{\rm H} = \dot{M}_\star + \dot{M}_{\rm ej}, \quad (10)$$

where $\dot{M}_{\rm ej}$ is the rate of ejection of gas mass by feedback and $f_{\rm b}$ is the baryon fraction relative to dark matter. Eqn. 10 can be rewritten in terms of the dimensionless mass loading factor, $\beta_{\rm ml} = \dot{M}_{\rm ej}/\psi$, yielding

$$f_{\rm b}\dot{M}_{\rm H} = \dot{M}_\star\,(1 + \beta_{\rm ml}/(1-R)), \quad (11)$$

where R is the fraction of gas recycled back into the ISM as a result of stellar evolution, which is assumed to be a constant so that $\dot{M}_\star = (1-R)\psi$. At this stage we note that supernova feedback in our fiducial GALFORM model is parametrised as $\beta_{\rm ml} \propto V_{\rm disk}^{-3.2}$ (see eqn. 2). Therefore, in the regime under consideration where $V_{\rm disk}$ does not evolve with time, $\beta_{\rm ml}$ is constant. In this regime, Eqn. 11 can be integrated to give

$$f_{\rm b}M_{\rm H} = M_\star\,(1 + \beta_{\rm ml}/(1-R)). \quad (12)$$

If we then substitute the scalings from eqns 8 and 9 into 12 and 11 and then divide 11 by 12, we find that the specific stellar mass assembly rate is given by

$$\frac{\dot{M}_\star}{M_\star} = \frac{\dot{M}_{\rm H}}{M_{\rm H}} = \frac{1}{t_{\rm age}}. \quad (13)$$

We note that Stringer et al. (2011) obtain the same result, where they argue that this behaviour is generic in the regime where the halo mass assembly process is approximately self-similar.

In Fig. 3, it can be seen that the evolution of the average specific star formation rates in our fiducial GALFORM model closely tracks the inverse of the age of the universe at a given epoch. By following the derivation of Eqn. 13, it can be seen that this behaviour will naturally emerge if $V_{\rm vir}$ and $\beta_{\rm ml}$ remain approximately constant with lookback time. We note that although this is true for the majority of the lifetimes of star forming galaxies in our fiducial model, Fig. 6 shows that the situation changes for $\beta_{\rm ml}$ at early times. This explains why the efficiency of converting accreted gas into stars, as shown in Fig. 5, rises rapidly at early times.

The derivation of Eqn. 13 ignores the reincorporation of gas after ejection by feedback. This is actually a very poor approximation given that Fig. 6 shows that $\beta_{\rm ml}$ is always $\gg 1$ over the lifetime of the galaxies which we consider. In addition, the bottom panel of Fig. 6 shows that the reincorporation timescale is typically between a factor of 6 and 20 shorter than the age of the universe. Combined, these two features of the model mean that gas reincorporation will be highly significant in shaping the predicted star formation histories of star forming galaxies. Therefore, it is clear that Eqn. 10 needs to be modified in order to account for the fact that the gas will typically have been recycled between the galaxy disk and the halo many times before forming into stars. To incorporate this effect, Eqn. 10 can be rewritten as

$$f_{\rm b}\dot{M}_{\rm H} + \dot{M}_{\rm ret} = \dot{M}_\star + \dot{M}_{\rm ej} = \dot{M}_\star\,(1 + \beta_{\rm ml}/(1-R)), \quad (14)$$

where the rate of return of gas from a reservoir of ejected gas of mass $M_{\rm res}$ is given by $\dot{M}_{\rm ret} = M_{\rm res}/t_{\rm ret}$. For the case where $\beta_{\rm ml} \gg 1$, Eqn. 14 simplifies to

$$f_{\rm b}\dot{M}_{\rm H} + \dot{M}_{\rm ret} \approx \dot{M}_\star \frac{\beta_{\rm ml}}{1-R} = \dot{M}_{\rm ej}. \quad (15)$$

The gas mass in the reservoir is given by

$$M_{\rm res} = \int_0^{t_{\rm age}} \left(\dot{M}_{\rm ej} - \dot{M}_{\rm ret}\right) {\rm d}t. \quad (16)$$

For the case where the halo mass accretion rate is approximately constant over a time scale, $t_{\rm age}$, substituting Eqn. 15 into 16 yields

$$M_{\rm res} \approx \int_0^{t_{\rm age}} f_{\rm b}\dot{M}_{\rm H}\,{\rm d}t \approx f_{\rm b}\dot{M}_{\rm H}\,t_{\rm age}. \quad (17)$$

Therefore, in this idealised case $\dot{M}_{\rm ret}$ can be written as

$$\dot{M}_{\rm ret} = M_{\rm res}/t_{\rm ret} \approx f_{\rm b}\dot{M}_{\rm H}\,\frac{t_{\rm age}}{t_{\rm ret}}. \quad (18)$$

Combining Eqns 18 and 15, we find that

$$f_{\rm b}\dot{M}_{\rm H}\left(1 + \frac{t_{\rm age}}{t_{\rm ret}}\right) \approx \dot{M}_\star \frac{\beta_{\rm ml}}{1-R}. \quad (19)$$

In GALFORM, the return timescale is parametrised as

$$t_{\rm ret} = \frac{t_{\rm dyn}}{\alpha_{\rm reheat}} = \frac{1}{\alpha_{\rm reheat}}\sqrt{\frac{3}{4\pi G\bar{\rho}_{\rm H}}}, \quad (20)$$

where $t_{\rm dyn} = R_{\rm vir}/V_{\rm vir}$ is the dynamical timescale of the halo

and $\alpha_{\rm reheat}$ is a dimensionless model parameter set to 1.26 for our fiducial model. As before, we can use Eqn. 7 and adopt the case of an $\Omega_{\rm M} = 1$ universe, yielding

$$t_{\rm ret} = \frac{t_{\rm age}}{2\pi\alpha_{\rm reheat}}. \quad (21)$$

Examination of the bottom panel of Fig. 6 shows that this is a reasonable approximation. Finally, combining eqns 21 and 19 yields

$$f_{\rm b}\dot{M}_{\rm H}(1 + 2\pi\alpha_{\rm reheat}) \approx \dot{M}_{\star}\frac{\beta_{\rm ml}}{1-R}. \quad (22)$$

Therefore, for the idealised case where $\beta_{\rm ml} \gg 1$, $t_{\rm cool} < t_{\rm ret}$, and $\dot{M}_{\rm H}$ remaining approximately constant over a time scale, $t_{\rm age}$, then the effect of including gas recycling is to increase the amount of gas available for star formation roughly by a factor of $1 + 2\pi\alpha_{\rm reheat}$. For our fiducial GALFORM model with $\alpha_{\rm reheat} = 1.26$, this factor is ~ 9. We note that this modulation factor is completely independent of galaxy stellar mass, provided $\beta_{\rm ml} \gg 1$. Finally, as Equation 22 is equivalent to Equation 11 multiplied by a constant factor, repeating the exercise of integrating Equation 22 will give the same result that the specific stellar mass assembly rate is simply given by $\dot{M}_{\star}/M_{\star} = 1/t_{\rm age}$, provided that $V_{\rm vir}$ remains constant with time.

5 TOWARDS REPRODUCING THE INFERRED STELLAR MASS ASSEMBLY HISTORIES OF STAR-FORMING GALAXIES

In Section 4 and Appendix B, we have demonstrated that for the standard parametrisations of supernova feedback, star formation and gas reincorporation used in GALFORM, it is not possible to reproduce the stellar mass assembly histories of star forming galaxies inferred from observations. The next logical step is to consider how these parametrisations would need to be changed in order to better reproduce the inferred observational trends. Clearly, the ideal scenario is to change the parametrisations such that they are more physically motivated and/or satisfy direct empirical constraints. The opposite and less desirable extreme is to use increasingly flexible parametrisations which have to be constrained statistically to reproduce global diagnostics of the galaxy population. Currently, the implementation of star formation in GALFORM can be argued to fall into the former case while the default implementations of feedback and reincorporation fall into the latter. We therefore choose to focus on how the implementation of feedback and gas reincorporation could be modified to change the model predictions relevant to our analysis.

5.1 Modifying the mass loading factor for supernova feedback

From the comparison between the predicted and inferred efficiency of stellar mass assembly shown in Fig. 5, it is clear that the degree of coevolution between stellar mass and halo mass assembly rates needs to be reduced in GALFORM in order to reproduce the trends we infer according to the observations. This requirement appears to be particularly pertinent from intermediate through to late times (roughly in the redshift range, $0 < z < 1$), where the efficiency of converting accreted gas into stars is inferred from the observations to drop after a peak at intermediate redshift. In Section 4.2, we demonstrated that the efficiency of feedback in our fiducial model, characterised by the mass loading factor, $\beta_{\rm ml}$, does not vary significantly over this redshift range. This is because the disk circular velocity does not evolve strongly over the lifetime of a typical star forming galaxy in GALFORM. A different parametrisation for $\beta_{\rm ml}$ that does not depend only on circular velocity could potentially change this behaviour.

Lagos et al. (2013) have recently introduced an alternative parametrisation for the ejection of gas from galaxy disks and bulges as a result of feedback from supernovae (see also Creasey et al. 2013). This offers a natural starting point for our investigation because their work is motivated on physical grounds. Briefly, their methodology is to track the evolution of bubbles driven by supernovae as they expand into the ambient ISM. They calculate the rate at which mass entrained in these bubbles escapes vertically out of the disk and find that $\beta_{\rm ml}$ cannot be naturally parametrised as a function of the disk circular velocity. Instead, they find that $\beta_{\rm ml}$ is better described as a function of the gas fraction in the disk, $f_{\rm g}$, and either the total gas surface density, $\Sigma_{\rm g}$, of the disk at the half mass radius, r_{50}, or the gas scaleheight, $h_{\rm g}$, of the disk at the half mass radius. From this point onwards we refer to the former as the surface density parametrisation and the latter as the scaleheight parametrisation. The surface density parametrisation is given by

$$\beta_{\rm ml} = \left[\frac{\Sigma_{\rm g}(r_{50})}{1600{\rm M}_{\odot}{\rm pc}^{-2}}\right]^{-0.6}\left[\frac{f_{\rm gas}}{0.12}\right]^{0.8}, \quad (23)$$

and the scaleheight parametrisation is given by

$$\beta_{\rm ml} = \left[\frac{h_{\rm g}(r_{50})}{15{\rm pc}}\right]^{1.1}\left[\frac{f_{\rm gas}}{0.02}\right]^{0.4}. \quad (24)$$

We have used both of these parametrisations as separate modifications to our fiducial model and find that neither significantly changes the shapes of the stellar mass assembly histories of star forming galaxies to the extent that the model predictions are brought into better agreement with the data. The reason for this failure is illustrated in Fig 7, where we compare the average evolution in $\beta_{\rm ml}$ for galaxies that are star forming and central at $z = 0$ between the different models. It can be seen that although the modifications change the overall normalisation of $\beta_{\rm ml}$ and the dependence on $M_{\star}(t_0)$, the modified models actually result in even less evolution of $\beta_{\rm ml}$ over the lifetime of a typical star forming galaxy. Further investigation shows that this outcome arises because the effect on $\beta_{\rm ml}$ caused by the decline in the surface densities of star forming galaxies as they evolve is cancelled out by a corresponding drop in the gas fractions.

5.2 Modifying the gas reincorporation timescale

In addition to the mass loading factor, $\beta_{\rm ml}$, the way that ejected gas is reincorporated back into haloes is also modelled in a phenomenological manner in GALFORM. Therefore, an alternative to modifying the mass loading factor supernova feedback in our model is to alter the timescale for gas reincorporation for gas that has been ejected, $t_{\rm ret}$. At this stage, we choose to revert to the default parametrisation of $\beta_{\rm ml}$ (which depends on circular velocity) at this stage because using the modified models from Lagos et al. (2013) would require substantial retuning of various model parameters to recover an agreement with the observed local luminosity and stellar mass functions.

In the third panel of Fig. 6, we show the ratio of the characteristic gas reincorporation timescale relative to the age of the universe

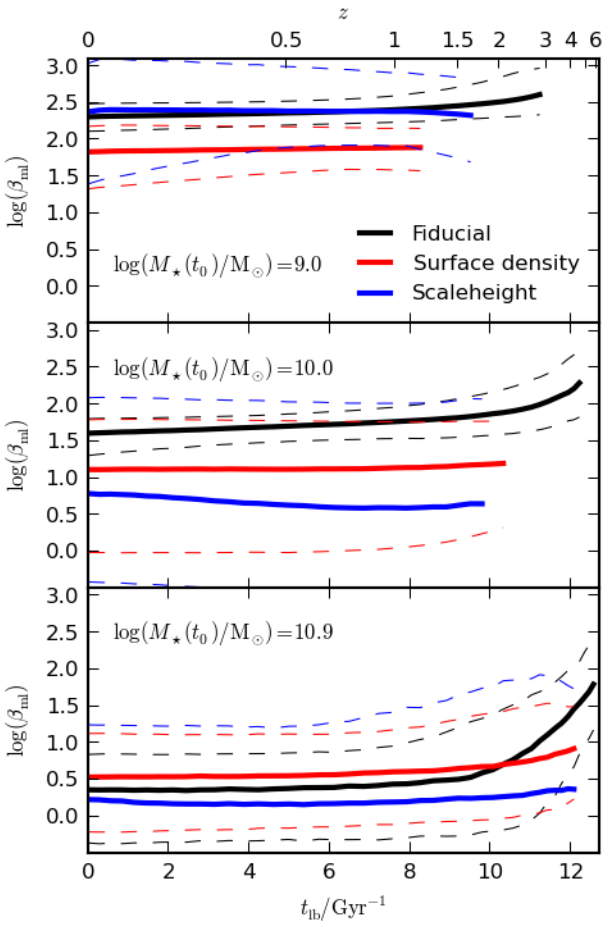

Figure 7. The average evolution in the mass loading factor of outflows, $\beta_{\rm ml}$, for model galaxies which are central and star forming at $z = 0$. Model galaxies are binned according to their $z = 0$ stellar mass, with each panel corresponding to a different mass bin. The median $z = 0$ stellar mass in each bin is labelled in each panel. Solid black lines show the mean mass loading factor from our fiducial GALFORM model. Dashed black lines show the corresponding median, $10^{\rm th}$ and $90^{\rm th}$ percentiles. Red lines show the same information but for a version of our fiducial model modified to use the surface density mass loading parametrisation, given by Eqn. 23 (Lagos et al. 2013). Blue lines show the same information but for a version of our fiducial model modified to use the scaleheight mass loading parametrisation, given by Eqn. 24.

as a function of lookback time for our fiducial model. As discussed in Section 4.2, this ratio of timescales evolves very little over the lifetime of a typical star forming galaxy, partly explaining the close levels of coevolution between stellar and halo mass assembly seen in Fig. 5 for our fiducial model. The most desirable step at this stage would be to formulate a physically motivated model for gas reincorporation timescales in the hope that a more realistic model could change this behaviour. Such an undertaking is beyond the scope of this study, but as an intermediate step, we instead introduce an *ad hoc* modification to the parametrisation of gas reincorporation timescales used in GALFORM. We note that this step essentially amounts to an empirical fit to the trends which we infer from the data and is of little scientific value in itself. However, the resulting evolution in the reincorporation timescale for star forming galaxies can serve as a guide for the development of a physically motivated model in future work.

To match the shape of the stellar mass assembly histories inferred from the data shown in Fig. 4, we consider a model where $t_{\rm age}/t_{\rm ret}$ rises from early times to a peak at $z = 2$, before falling to $z = 0$. A natural way to achieve an early time rise is to make $t_{\rm age}/t_{\rm ret}$ correlate positively with halo mass. This is the same scaling that Henriques et al. (2013) adopt in order to allow their model to reproduce the observed evolution in the stellar mass function. However, a natural scaling that results in a drop in $t_{\rm age}/t_{\rm ret}$ at late times is less obvious and we instead choose to simply introduce an arbitrary function of redshift to achieve this. After a process of experimentation and iteration, we arrive at the following modified parametrisation for gas reincorporation,

$$\dot{M}_{\rm hot} = \frac{\alpha_{\rm reheat}}{t_{\rm dyn}} \left(\frac{M_{\rm H}}{10^{11.9}{\rm M}_{\odot}} \right) f(z), \qquad (25)$$

where $f(z)$ is given by

$$\log[f(z)] = 6 \, \exp \left[-\frac{(1+z)}{3} \right] \log[1+z]. \qquad (26)$$

At this stage we note that in Appendix B, we show that the shapes of the stellar mass assembly histories predicted by GALFORM are almost invariant under changes in the model parameters which control the relationship between stellar and halo mass. In other words, this means that until now, our results for the shape of the stellar mass assembly histories of star forming galaxies have been independent of whether or not the model provides a good match to the $z = 0$ stellar mass function. However, once we change the parametrisation of the gas reincorporation in GALFORM, this feature of the model may not be preserved. Consequently, we now have to consider whether our modified GALFORM models can also reproduce the $z = 0$ stellar mass function, particularly because we have introduced a dependence on halo mass into Eqn. 25. We find that we can recover reasonable agreement with the local stellar mass function simply by fine tuning the various model parameters that appear in Eqn. 25. We also reduce the threshold for AGN feedback to be effective at suppressing gas cooling in haloes by changing the model parameter $\alpha_{\rm cool}$ from 1.0 to 1.3 (see Bower et al. 2006). From this point onwards, we refer to this modified model simply as the modified reincorporation model.

A comparison between our fiducial model and the modified reincorporation model for the evolution in $t_{\rm ret}/t_{\rm age}$ for star forming galaxies is presented in Fig. 8. In addition, Fig. 8 also shows the corresponding timescale proposed by Henriques et al. (2013) which scales only with the virial mass. By construction, $t_{\rm ret}/t_{\rm age}$ evolves much more strongly in our modified reincorporation model than in our fiducial model. Additionally, the dispersion in $t_{\rm ret}/t_{\rm age}$ can be slightly larger in the modified model for some lookback times. Given that Eqn. 25 introduces a dependence on halo mass, the change is presumably caused by scatter in the relationship between the stellar mass and halo mass of central star forming galaxies. This is noteworthy because any change in the scatter in $t_{\rm ret}/t_{\rm age}$ could have an effect on the scatter of the star forming sequence predicted by our modified reincorporation model.

The evolution in the cooling timescale is also shown in Fig. 8. It can be seen that for our modified reincorporation model, the cooling timescale can become significantly longer than the reincorporation timescale for the most star forming galaxies. In this regime, gas that is rapidly reincorporated back into the halo will be delayed from returning to the galaxy disk until the gas is able to cool. This is important because further shortening the reincorporation timescale

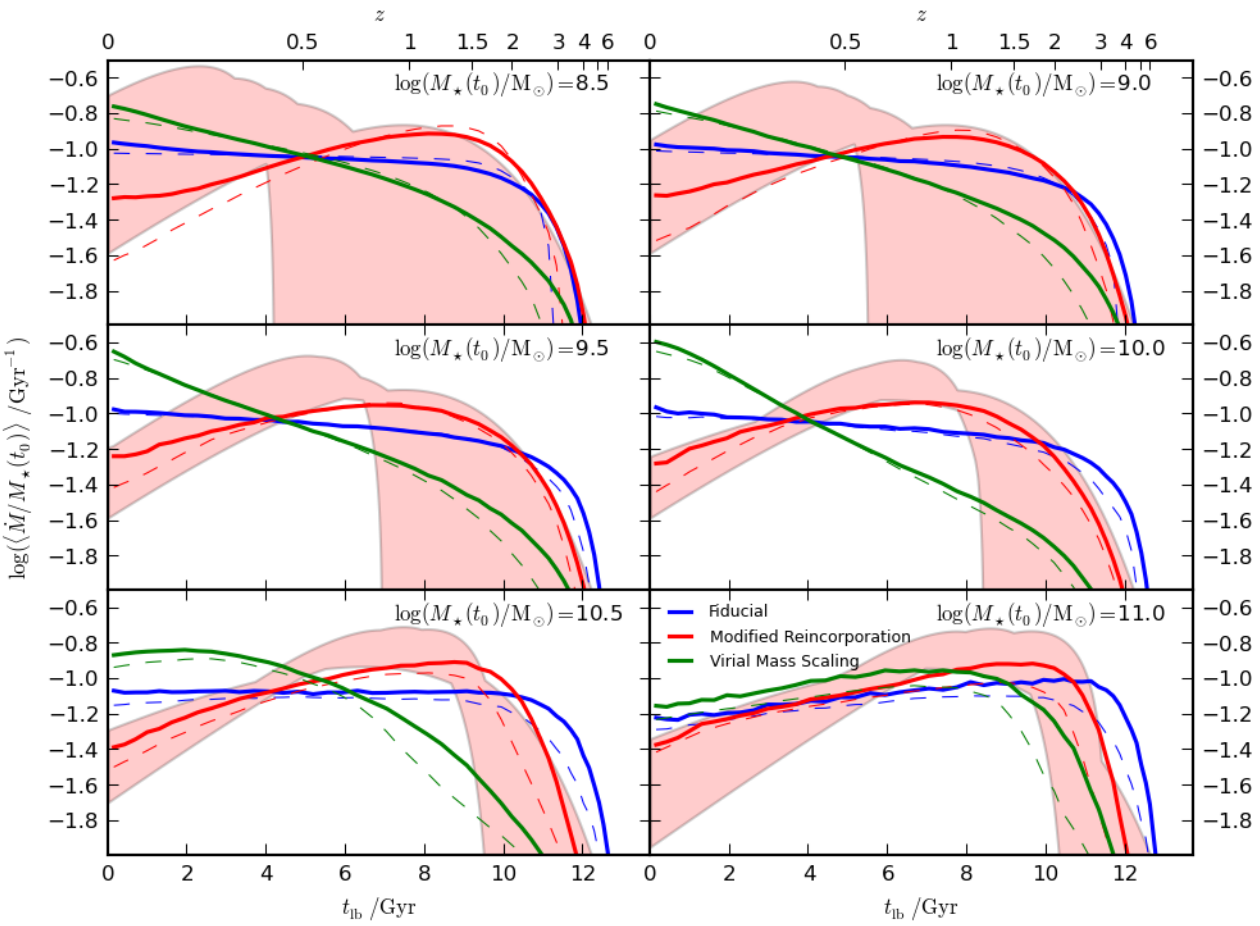

Figure 9. The average stellar mass assembly histories of galaxies that are star forming at $z = 0$, plotted as a function of lookback time. Blue solid lines show predictions from our fiducial GALFORM model for the mean mass assembly histories of the main stellar progenitors of central galaxies. Dashed blue lines show the corresponding medians of the distribution. Red lines show the same information but for the modified reincorporation model. Green lines show the same information but for a model using the virial mass scaling for the reincorporation timescale proposed by Henriques et al. (2013). Model galaxies are binned according to their $z = 0$ stellar mass with each panel corresponding to a different mass bin. The median $z = 0$ stellar mass in each bin is labelled in each panel. The filled pink region shows the range of stellar mass assembly histories that are inferred by applying the MSI technique to observational data from the literature.

in this regime will cease to have a significant impact on the rate at which gas is made available for star formation.

A comparison between our fiducial model and the modified reincorporation model for the predicted stellar mass assembly histories of star forming galaxies is presented in Fig. 9. Again, by construction we have tuned the modified reincorporation model in order to ensure qualitative agreement with the pink shaded region inferred from the observations using MSI. Comparison with the stellar mass assembly histories inferred from observational data shown in Fig. A5 shows that this agreement holds with MSI applied to observational data where the slope of the star forming sequence, $\beta_{\mathrm{sf}} \approx 0$. As discussed in Section 4.1, a lower value of β_{sf} introduces a strong downsizing trend into the stellar mass assembly histories of star forming galaxies which is difficult to reconcile with the approximately self-similar shape of the halo mass assembly histories predicted by the ΛCDM cosmological model. In principle, we could adjust Eqn. 25 even further to try to reproduce this downsizing trend. However, we have already introduced a very strong redshift scaling into the reincorporation timescale. Therefore, we choose to present a modified model which is closest to our fiducial model while still showing consistency with the pink shaded region in Fig. 9.

Finally, we show the comparison between our fiducial model and the modified reincorporation model for the evolution in the specific star formation rates of star forming galaxies in Fig. 3. Our modification to the reincorporation timescale has mixed success. For the top two panels, corresponding to the $\log(M_\star/\mathrm{M}_\odot) = 9.5, 10$ bins, the modified model shows a significantly improved agreement with the observational trend. Unlike for the fiducial model, the evolution in the mean specific star formation rates in the modified model does not trace the inverse of the age of the Universe as a function of lookback time. Instead, specific star formation rates are elevated at early times before dropping below the fiducial model at $z < 0.5$. For the $\log(M_\star/\mathrm{M}_\odot) = 10.5$ bin, the modified reincorporation model has a steeper drop below $z \approx 0.5$ compared to the fiducial model but the two models are very similar at higher redshifts, in disagreement with the data. The two models are very similar for all lookback times in the $\log(M_\star/\mathrm{M}_\odot) = 11$ bin and are both in disagreement with the data.

At first glance it is puzzling that modified reincorporation

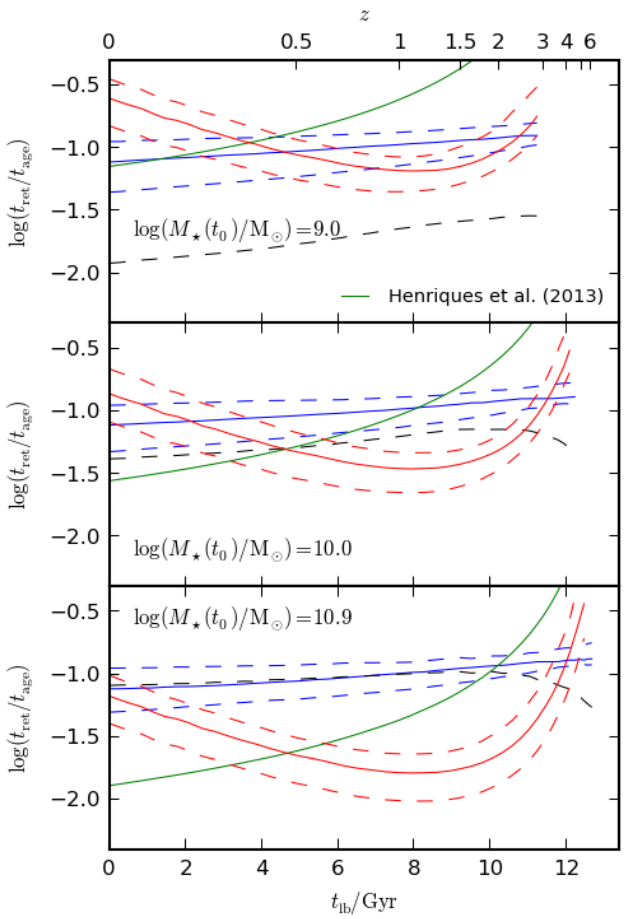

Figure 8. The ratio of the average reincorporation timescale to the age of the universe for model galaxies which are central and star forming at $z = 0$, plotted as a function of lookback time. Model galaxies are binned according to their $z = 0$ stellar mass and each panel shows a different stellar mass bin. The median $z = 0$ stellar mass in each bin is labelled in each panel. Solid blue lines show the medians of the distribution from our fiducial GALFORM model. Dashed blue lines show the corresponding $10^{\rm th}$ and $90^{\rm th}$ percentiles. Red lines show the same information but for the modified reincorporation model. Green solid lines show the median of the distribution for galaxies from our fiducial model which would be obtained if we were to use the reincorporation timescale from eqn. 8 in Henriques et al. (2013). For reference, black dashed lines show the ratio of the median cooling timescale, $t_{\rm cool}$, to the age of the universe for model galaxies from our fiducial model.

model fails to reconcile the model predictions with the observational data for massive star forming galaxies while it does qualitatively reproduce the inferred stellar mass assembly histories shown in Fig. 9. However, it must be kept in mind that our modification to the reincorporation timescale was constructed only to reproduce the shape of the stellar mass assembly histories of galaxies that are still star forming at $z = 0$. Galaxies observed at $z > 0$ in the most massive stellar mass bins shown in Fig. 3 will, typically, have dropped below the star forming sequence by $z = 0$. Therefore, the specific star formation rates of the most massive galaxies at high redshift will not have been constrained by our analysis of stellar mass assembly histories of galaxies that are still star forming at $z = 0$. Furthermore, galaxies that are quenched above $z \approx 1 - 2$ will be less affected by the rapid evolution in the reincorporation timescale which we impose in Eqn. 26 below $z = 2$. This highlights the need for a physical model of gas reincorporation rather than the artificial redshift scaling which we use here. In addition, for the most massive star forming galaxies, we show in Fig. 8 that the cooling timescales become long relative to the modified reincorporation timescales. As discussed earlier, this will reduce the impact of any modification towards shorter reincorporation timescales. Finally, the mass loading factor, $\beta_{\rm ml}$, for the most massive galaxies is smaller than for lower mass galaxies. Therefore, a larger fraction of gas accreted onto the haloes of these systems for the first time will be able to form stars without being affected by the reincorporation timescale.

Fig. 9 and Fig. 3 also show the stellar mass assembly histories and specific star formation rate evolution predicted by an alternative GALFORM model that uses the virial mass scaling for the reincorporation timescale proposed by Henriques et al. (2013). Details of this model and a discussion of the differences with our modified reincorporation model are presented in Appendix C. To summarise, we find that this alternative model with the virial mass scaling is considerably more successful than either our fiducial model or our modified reincorporation model in reproducing the observed evolution in the stellar mass function. However, Fig. 9 and Fig. 3 show that this alternative model fails to reproduce the stellar mass assembly and star formation rate evolution inferred from observations. We strongly emphasise that this result will not necessarily hold for the Henriques et al. (2013) model where the treatment of gas that is ejected from galaxy disks differs from the GALFORM model.

6 DISCUSSION

The focus of this study has been on using the observed evolution of the star forming sequence as a constraint on galaxy formation models. The disagreement in this evolution between models and observational data is undoubtedly related to the problems with reproducing the correct evolution in the low mass end of the stellar mass function which has recently received considerable attention in the literature (e.g. Avila-Reese et al. 2011; Weinmann et al. 2012; Henriques et al. 2013; Lu et al. 2013a,b). Specifically, there is a general finding that models and simulations overpredict the ages of low mass galaxies and consequently underpredict evolution in the low mass end of the stellar mass function at low redshift. Weinmann et al. (2012) interpret this problem as an indication that the level of coevolution between halo and stellar mass assembly needs to be reduced, broadly in agreement with our results. However, part of the reason why they arrive at this conclusion is because they identify the prediction of a positive correlation between specific star formation rate and stellar mass as a key problem with respect to the data. We note that in contrast, GALFORM naturally predicts a slightly negative correlation for star forming galaxies and that this is also true for many other models and simulations presented in the literature (e.g. Santini et al. 2009; Dutton et al. 2010; Lamastra et al. 2013; Torrey et al. 2014).

Henriques et al. (2013) show that there is no combination of parameters for their standard galaxy formation model that can reconcile the model with the observed evolution in the stellar mass and luminosity functions. This is consistent with the findings of Lu et al. (2013a), who use a similar methodology but for a different model. Lu et al. (2013b) compare three different models of galaxy formation and find that they all predict very similar stellar mass assembly histories and suffer from predicting too much star formation at high redshift in low mass haloes. We note that the models presented in

Lu et al. (2013b) are all very similar to GALFORM in many respects and that therefore the similarity of the predictions from their three models makes sense in the context of the discussion we present in Appendix B.

Henriques et al. (2013) go one step further to suggest an empirical modification to the reincorporation timescale within their model that reduces the rate of star formation at early times in low mass haloes. In this respect, their equation 8 uses the same scaling between reincorporation timescale and halo mass which we introduce in Eqn. 25 for the same reason. However, our modification diverges from their suggestion in that we also require an additional redshift dependence that lengthens the reincorporation timescale towards low redshift. The modification suggested by Henriques et al. (2013) can be compared to our modification in Fig. 8. The difference between the two suggested modifications stems from the way that our analysis indicates that it is not simply that stars form too early in the model. Instead, we find that it is the precise shape of the stellar mass assembly history which is inconsistent with the currently available data which favours a peak of activity at intermediate times. This highlights how the differences in methodology between different studies can lead to different conclusions. Our analysis is designed to reduce the number of relevant physical processes by focusing only on the normalisation of the star forming sequence. In principle, this approach can provide a more direct insight into how the implementation of different physical processes within galaxy formation models needs to be changed, provided that the uncertainty in the relevant observations can be correctly accounted for. On the other hand, as discussed in Appendix C, our modified reincorporation model does not reproduce the evolution in the stellar mass function inferred from recent observations. We again emphasise that the focus of this study is on the evolution of the normalisation of the star forming sequence and that the stellar mass function can be affected by the quenching processes which we have not considered in our analysis. Nonetheless, it may well be the case that our methodology is limited by the lack of a consensus on the slope of the star forming sequence in observations. Alternatively, there could be some inconsistency between observations of the star forming sequence and observations of the evolution in the stellar mass function. We note that the latter possibility is disfavoured by recent abundance matching results (e.g. Behroozi et al. 2013; Moster et al. 2013).

6.1 Do the stellar mass assembly histories of star forming galaxies rise and then fall?

Our suggestion that the reincorporation timescale needs to be increased at low redshift stems from our inference from observations that the stellar mass assembly histories of star forming galaxies rise to a peak before falling towards the present day. As discussed in Appendix A3, this inference is consistent with the findings of Leitner (2012) who use a similar methodology, albeit with the caveat that we find that evidence of a strong downsizing trend in the purely star forming population is not conclusive. Instead, we find that the considerable uncertainty that remains in the power-law slope of the star forming sequence means that overall, the observational data are also consistent with no downsizing, such that the shapes of the stellar mass assembly histories of star forming galaxies are independent of the final stellar mass. Clearly, any improvements in measuring the form of the star forming sequence as a function of lookback time would greatly increase the constraining power of the MSI technique with respect to galaxy formation models. If the slope of the sequence, $\beta_{\rm sf}$, can be conclusively shown to be significantly below zero as advocated, for example by Karim et al. (2011), then even larger modifications than those considered here towards separating stellar and halo mass assembly would be required.

Another methodology that can be used to infer the shape of the stellar mass assembly histories of galaxies is to employ abundance matching to make an empirical link between the dark matter halo population predicted by theory and the observed galaxy population (e.g. Behroozi et al. 2013; Moster et al. 2013; Yang et al. 2013). Comparison with stellar mass assembly histories of the star forming galaxies that are discussed in this study is complicated by the fact that abundance matching has only been used so far to predict the average star formation histories of all galaxies (including passive galaxies) and as a function of halo mass. On average, the haloes hosting the galaxies which we consider in this study have median masses of $\log(M_{\rm H}/{\rm M}_{\odot}) < 12$, where the fraction of passive central galaxies relative to star forming centrals is predicted to be negligible. However, because there is substantial scatter between stellar mass and halo mass for central galaxies, the fraction of passive galaxies at a given stellar mass is not negligible for most of the stellar mass bins which we consider in this study. For example, the fraction of central galaxies with $\log(M_{\star}/{\rm M}_{\odot}) = 10$ that are passive is predicted to be 25% at $z = 0$ in our fiducial GALFORM model. Furthermore, the star forming galaxies considered in this study and in Leitner (2012) are hosted by haloes that reside within a fairly narrow range of halo mass. If we ignore these issues, then qualitatively speaking, it is apparent that the shape of stellar mass assembly histories inferred by Behroozi et al. (2013) and Yang et al. (2013) are broadly consistent with what we and Leitner (2012) infer from the data, in that there is a rise with time towards a peak at some intermediate redshift before a fall towards the present day. Moster et al. (2013) show qualitative agreement with this picture for $\log(M_{\rm H}/{\rm M}_{\odot}) = 12$ haloes, but find a constant rise from early to late times in the stellar mass assembly rates of galaxies that reside within haloes with $\log(M_{\rm H}/{\rm M}_{\odot}) = 11$.

Finally, we also note that Pacifici et al. (2013) find that the spectral energy distributions (SEDs) of massive star forming galaxies are well described by models that feature initially rising then declining star formation histories. However, for lower mass galaxies they find that the SEDs are best reproduced using star formation histories that monotonically rise towards the present day, in qualitative agreement with the results from Moster et al. (2013). However, their galaxy sample does not include any galaxies observed below $z = 0.2$, corresponding to a lookback time of $t_{\rm lb} \approx 3\,{\rm Gyr}$. It is therefore unclear whether their analysis disfavours a drop in the star formation rates of lower mass galaxies at late times.

6.2 Modifications to galaxy formation models

The parametrisations for star formation and feedback that are implemented in most galaxy formation models can reproduce the shape of the local luminosity and stellar mass functions. However, as observational data that characterises the evolution of the galaxy population has improved, it has now been demonstrated that either one or more of these parametrisations is inadequate or alternatively that another important physical process has been neglected in the models entirely. The assumption that the reincorporation timescale for ejected gas scales with the dynamical timescale of the host halo is common to various semi-analytic galaxy formation models (e.g. Bower et al. 2006; Croton et al. 2006; Somerville et al. 2008; Lu et al. 2011). If the reincorporation timescale is set to exactly the dynamical timescale, the associated physical assumption is that ejected gas simply behaves in a ballistic manner, ignoring any pos-

sible hydrodynamical interaction between the ejected gas and the larger scale environment. In practice, these models (including ours) typically introduce a model parameter such that the reincorporation timescale is not exactly equal to the dynamical timescale, reflecting the considerable uncertainty on predicting this timescale. Nonetheless, the assumption that this uncertainty can be represented by a single parameter and that there is no additional scaling with other galaxy or halo properties is clearly naive. Comparison with hydrodynamical simulations will clearly be useful in this respect, provided that the reincorporation rates can be clearly defined and measured from the simulations and that the effect of the assumptions made in sub-grid feedback models can be understood.

While we and Henriques et al. (2013) show that a modification to the reincorporation timescale for gas ejected by feedback can be one solution, we could equally change the parametrisation for the mass loading factor, $\beta_{\rm ml}$, or the star formation law introduced in Lagos et al. (2011b). In this analysis, we found that the physically motivated parametrisation for the mass loading factor of SNe driven winds presented in Lagos et al. (2013) fails to reconcile the model with the data. However, it should be noted that unlike the fiducial model we consider for this study, the supernova feedback model presented in Lagos et al. (2013) relies heavily upon correctly predicting the evolution in the sizes of galaxies. In principle, if the predicted sizes evolved differently in our model, it is possible that using the Lagos et al. (2013) supernova feedback model could help to reconcile model predictions for the stellar mass assembly histories of galaxies with the observational data. As for modifying the star formation law, the implementation used in GALFORM is derived from direct empirical constraints. Furthermore, changing the star formation law will have little impact on the stellar mass assembly histories of star forming galaxies as long as the characteristic halo accretion timescale is longer than the disk depletion timescale. Of course, an alternative to the physically motivated Lagos et al. (2013) model is simply to implement an ad hoc modification to the mass loading, similar to that given by Eqn. 25 for the reincorporation timescale. We note that by doing this, we find it is possible to produce a model that almost exactly matches the predictions made by the modified reincorporation model presented in this paper. It therefore suffers from the same problems as the modified reincorporation model in reproducing the observed evolution of the stellar mass function and the decline in the specific star formation rates of the most massive star forming galaxies at a given redshift.

Many other suggestions for changing the stellar mass assembly histories predicted by models and simulations have been made recently in the literature, typically focusing on reducing the fraction of stars that form at high redshift. For example, Krumholz & Dekel (2012) argue that early star formation is reduced once the dependence of star formation on metallicity is properly implemented in hydrodynamical simulations. Gabor & Bournaud (2014) suggest that if galaxies at high redshift accrete directly from cold streams of gas, the accreted gas injects turbulent energy into galaxy disks, increasing the vertical scaleheight and consequently lowering the star formation efficiency in these systems by factors of up to 3. Lu et al. (2014) demonstrate that if the circum-halo medium can be preheated at early times up to a certain entropy level, the accretion of baryons onto haloes can be delayed, reducing the amount of early star formation. Various authors (e.g Aumer et al. 2013; Stinson et al. 2013; Trujillo-Gomez et al. 2013) find that implementing a coupling between the radiation emitted by young stars and the surrounding gas into their simulations can significantly reduce the levels of star formation in high redshift galaxies. Hopkins et al. (2013a) and Hopkins et al. (2013b) echo these findings and emphasise the highly non-linear nature of the problem once sufficient resolution is obtained to start resolving giant molecular cloud structures. They argue that radiative feedback is essential to disrupt dense star forming gas before SNe feedback comes into effect to heat and inject momentum into lower density gas, avoiding the overcooling problem as a result. It remains to be seen at this stage whether the emergent behaviour from such simulations, once averaged over an entire galaxy disk or bulge, can be captured in the parametrisations that are used in semi-analytic galaxy formation models.

7 SUMMARY

We have performed a detailed comparison between predictions from the GALFORM semi-analytic model of galaxy formation with observational data that describe the average star formation rates of star forming galaxies as a function of stellar mass and lookback time. To better understand the origin of discrepancies between the model and the data, we also use the observational data to infer the shape of the stellar mass assembly histories of galaxies that are still central and star forming at the present day. This is achieved by integrating the inferred relationship between star formation rate and stellar mass for star forming galaxies back in time from the present day. Crucially, we account for the considerable uncertainty that remains in the literature regarding the slope of the power-law dependence of star formation rate on stellar mass. We then attempt to explain our results by analysing the timescales of the various physical processes in the model which are important for shaping the stellar mass assembly histories of star forming galaxies.

Our main results are summarised as follows:

- For our fiducial model, there are qualitative differences with the observational data in the way that the average specific star formation rates of star forming galaxies evolve with time at a given stellar mass. The model predicts average specific star formation rates that evolve too slowly with lookback time, tracing the inverse of the age of the universe at a given epoch. In contrast the observational data implies that the average specific star formation rates of star forming galaxies grow exponentially as a function of lookback time. Quantitatively, this leads to discrepancies in the predicted average specific star formation rates of up to $0.5\,{\rm dex}$ compared to the data.
- We show that the main sequence integration technique, as advocated by Leitner (2012), can qualitatively recover the shape of the stellar mass assembly histories of galaxies that are still star forming at the present day when it is applied to our fiducial model.
- After applying this technique to a compilation of observational data, we show that there is a qualitative difference between the inferred shape of the stellar mass assembly histories of star forming galaxies and the predictions from our fiducial model. Specifically, the model predicts stellar mass assembly histories that are almost flat over most of the lifetime of star forming galaxies. In contrast, the trend we infer from the data is that stellar mass assembly histories rise from early times, peak at an intermediate redshift and subsequently fall towards the present day.
- The exact position of the peak in these inferred stellar mass assembly histories depends sensitively on the slope of the star forming sequence of galaxies. We show that no clear consensus on this slope has emerged yet from observations presented in the literature. For the case where the specific star formation rate is independent of stellar mass, the resulting shape of the stellar mass assembly histories of galaxies that are still star forming at the present day

is also independent of stellar mass. For the case where there is a strong anti-correlation between specific star formation rate and stellar mass, there is also a strong downsizing trend that emerges for this population of galaxies. In this case, less massive galaxies start forming stars at a later time with respect to more massive star forming galaxies. We emphasise that this should be completely independent of processes that quench star formation in galaxies. Such a downsizing trend in the purely star forming population is difficult to reconcile with the approximately self-similar halo mass assembly histories predicted by simulations of structure formation.

- The shapes of the stellar mass assembly histories predicted by our fiducial model are unaffected by changes to the various input parameters to the GALFORM model. This is despite the fact that for the same changes to these model parameters, it is possible to significantly affect the present day relationship between stellar mass and halo mass.
- The roughly flat stellar mass assembly histories predicted by our fiducial model arise because of the standard parametrisations for supernova feedback that are implemented in semi-analytic galaxy formation models. The efficiency with which cold gas is ejected from galaxy disks evolves very little over the majority of the lifetimes of star forming galaxies. This comes as a result of the standard scheme used in semi-analytic models where the mass loading factor is a parametrised as a function of circular velocity which, in turn, is almost constant over the lifetime of an individual star forming galaxy. Similarly, the timescale, relative to the age of the Universe, over which gas ejected by feedback is reincorporated into galaxy haloes also varies very little for individual star forming galaxies. In this case, the typical assumption that the reincorporation timescale scales with the halo dynamical time results in this behaviour. We also show using simple arguments that when the efficiency of feedback does not vary with time for a given galaxy, the specific star formation rates of star forming galaxies will naturally trace the inverse of the age of the Universe at a given stellar mass.

We demonstrate that a modification to the reincorporation timescale, such that this timescale is lengthened at early and late times, can produce peaked stellar mass assembly histories for galaxies that are still star forming at the present day. This modification significantly improves the agreement with the data for the evolution in the average specific star formation rates of star forming galaxies with $9.5 < \log(M_\star/\mathrm{M}_\odot) < 10.0$. However, the modification is less effective for more massive star forming galaxies where radiative cooling timescales become comparable to or longer than the corresponding reincorporation timescales. We also show that the modification fails to reproduce the rapid evolution in the low mass end of the stellar mass function inferred from observations below $z = 2$.

We conclude that modifications to the standard implementations of supernova feedback used in galaxy formation models and cosmological hydrodynamical simulations are probably required. Rather than altering the efficiency of feedback or star formation in a global sense over the lifetime of a given galaxy, it appears to be necessary to introduce a dependency that changes the efficiency of one or both of these processes with time.

ACKNOWLEDGEMENTS

This work was supported by the Science and Technology Facilities Council [grant numbers ST/J501013/1, ST/F001166/1]. This work used the DiRAC Data Centric system at Durham University, operated by the Institute for Computational Cosmology on behalf of the STFC DiRAC HPC Facility (www.dirac.ac.uk). This equipment was funded by BIS National E-infrastructure capital grant ST/K00042X/1, STFC capital grant ST/H008519/1, and STFC DiRAC Operations grant ST/K003267/1 and Durham University. DiRAC is part of the National E-Infrastructure. We thank Violeta Gonzalez-Perez for making suggestions which helped improve the clarity of this paper.

REFERENCES

Aumer M., White S. D. M., Naab T., Scannapieco C., 2013, MNRAS, 434, 3142
Avila-Reese V., Colín P., González-Samaniego A., Valenzuela O., Firmani C., Velázquez H., Ceverino D., 2011, ApJ, 736, 134
Baldry I. K. et al., 2012, MNRAS, 421, 621
Bauer A. E. et al., 2013, MNRAS, 434, 209
Baugh C. M., 2006, Reports on Progress in Physics, 69, 3101
Behroozi P. S., Wechsler R. H., Conroy C., 2013, ApJ, 770, 57
Benson A. J., 2010, Phys. Rep., 495, 33
Benson A. J., Bower R., 2010, MNRAS, 405, 1573
Benson A. J., Bower R. G., Frenk C. S., Lacey C. G., Baugh C. M., Cole S., 2003, ApJ, 599, 38
Bernardi M., Meert A., Sheth R. K., Vikram V., Huertas-Company M., Mei S., Shankar F., 2013, MNRAS, 436, 697
Blitz L., Rosolowsky E., 2006, ApJ, 650, 933
Bouwens R. J. et al., 2012, ApJ, 754, 83
Bower R. G., Benson A. J., Malbon R., Helly J. C., Frenk C. S., Baugh C. M., Cole S., Lacey C. G., 2006, MNRAS, 370, 645
Bower R. G., Vernon I., Goldstein M., Benson A. J., Lacey C. G., Baugh C. M., Cole S., Frenk C. S., 2010, MNRAS, 407, 2017
Brinchmann J., Charlot S., White S. D. M., Tremonti C., Kauffmann G., Heckman T., Brinkmann J., 2004, MNRAS, 351, 1151
Ciambur B. C., Kauffmann G., Wuyts S., 2013, MNRAS, 432, 2488
Cole S., Lacey C. G., Baugh C. M., Frenk C. S., 2000, MNRAS, 319, 168
Creasey P., Theuns T., Bower R. G., 2013, MNRAS, 429, 1922
Croton D. J. et al., 2006, MNRAS, 365, 11
Daddi E., Cimatti A., Renzini A., Fontana A., Mignoli M., Pozzetti L., Tozzi P., Zamorani G., 2004, ApJ, 617, 746
Daddi E. et al., 2007, ApJ, 670, 156
Damen M., Labbé I., Franx M., van Dokkum P. G., Taylor E. N., Gawiser E. J., 2009, ApJ, 690, 937
Davé R., 2008, MNRAS, 385, 147
De Lucia G., Kauffmann G., White S. D. M., 2004, MNRAS, 349, 1101
Drory N., Alvarez M., 2008, ApJ, 680, 41
Dutton A. A., van den Bosch F. C., Dekel A., 2010, MNRAS, 405, 1690
Elbaz D. et al., 2007, A&A, 468, 33
Elbaz D. et al., 2011, A&A, 533, A119
Fakhouri O., Ma C.-P., Boylan-Kolchin M., 2010, MNRAS, 406, 2267
Feulner G., Goranova Y., Drory N., Hopp U., Bender R., 2005, MNRAS, 358, L1
Firmani C., Avila-Reese V., Rodríguez-Puebla A., 2010, MNRAS, 404, 1100
Font A. S. et al., 2008, MNRAS, 389, 1619
Gabor J. M., Bournaud F., 2014, MNRAS, 437, L56
Genel S. et al., 2014, ArXiv e-prints

González V., Bouwens R., Illingworth G., Labbé I., Oesch P., Franx M., Magee D., 2014, ApJ, 781, 34
Gunn J. E., Gott, III J. R., 1972, ApJ, 176, 1
Guo Q., Cole S., Eke V., Frenk C., Helly J., 2013, MNRAS, 434, 1838
Guo Q. et al., 2011, MNRAS, 413, 101
Heinis S. et al., 2014, MNRAS, 437, 1268
Henriques B. M. B., White S. D. M., Thomas P. A., Angulo R. E., Guo Q., Lemson G., Springel V., 2013, MNRAS, 431, 3373
Hirschmann M. et al., 2013, MNRAS, 436, 2929
Hopkins A. M., Beacom J. F., 2006, ApJ, 651, 142
Hopkins P. F., Cox T. J., Hernquist L., Narayanan D., Hayward C. C., Murray N., 2013a, MNRAS, 430, 1901
Hopkins P. F., Keres D., Onorbe J., Faucher-Giguere C.-A., Quataert E., Murray N., Bullock J. S., 2013b, ArXiv e-prints
Huang S., Haynes M. P., Giovanelli R., Brinchmann J., 2012, ApJ, 756, 113
Ilbert O. et al., 2013, A&A, 556, A55
Ilbert O. et al., 2010, ApJ, 709, 644
Jiang L., Helly J. C., Cole S., Frenk C. S., 2014, MNRAS, 440, 2115
Kannan R., Stinson G. S., Macciò A. V., Brook C., Weinmann S. M., Wadsley J., Couchman H. M. P., 2014, MNRAS, 437, 3529
Karim A. et al., 2011, ApJ, 730, 61
Koyama Y. et al., 2013, MNRAS, 434, 423
Krumholz M. R., Dekel A., 2012, ApJ, 753, 16
Labbé I. et al., 2010, ApJ, 716, L103
Lagos C. D. P., Baugh C. M., Lacey C. G., Benson A. J., Kim H.-S., Power C., 2011a, MNRAS, 418, 1649
Lagos C. d. P., Bayet E., Baugh C. M., Lacey C. G., Bell T. A., Fanidakis N., Geach J. E., 2012, MNRAS, 426, 2142
Lagos C. d. P., Lacey C. G., Baugh C. M., 2013, MNRAS, 436, 1787
Lagos C. D. P., Lacey C. G., Baugh C. M., Bower R. G., Benson A. J., 2011b, MNRAS, 416, 1566
Lamastra A., Menci N., Fiore F., Santini P., 2013, A&A, 552, A44
Leitner S. N., 2012, ApJ, 745, 149
Leitner S. N., Kravtsov A. V., 2011, ApJ, 734, 48
Li C., White S. D. M., 2009, MNRAS, 398, 2177
Lilly S. J., Le Fevre O., Hammer F., Crampton D., 1996, ApJ, 460, L1
Lin L. et al., 2012, ApJ, 756, 71
Lu Y., Mo H. J., Lu Z., Katz N., Weinberg M. D., 2013a, ArXiv e-prints
Lu Y., Mo H. J., Wechsler R. H., 2014, ArXiv e-prints
Lu Y., Mo H. J., Weinberg M. D., Katz N., 2011, MNRAS, 416, 1949
Lu Y. et al., 2013b, ArXiv e-prints
Madau P., Ferguson H. C., Dickinson M. E., Giavalisco M., Steidel C. C., Fruchter A., 1996, MNRAS, 283, 1388
Magdis G. E., Rigopoulou D., Huang J.-S., Fazio G. G., 2010, MNRAS, 401, 1521
Merson A. I. et al., 2013, MNRAS, 429, 556
Mitchell P. D., Lacey C. G., Baugh C. M., Cole S., 2013, MNRAS, 435, 87
Mortlock A., Conselice C. J., Bluck A. F. L., Bauer A. E., Grützbauch R., Buitrago F., Ownsworth J., 2011, MNRAS, 413, 2845
Moster B. P., Naab T., White S. D. M., 2013, MNRAS, 428, 3121
Moustakas J. et al., 2013, ApJ, 767, 50
Mutch S. J., Poole G. B., Croton D. J., 2013, MNRAS, 428, 2001
Muzzin A. et al., 2013a, ApJ, 777, 18
Muzzin A. et al., 2013b, ApJS, 206, 8
Noeske K. G. et al., 2007a, ApJ, 660, L47
Noeske K. G. et al., 2007b, ApJ, 660, L43
Obreja A., Brook C. B., Stinson G., Domínguez-Tenreiro R., Gibson B. K., Silva L., Granato G. L., 2014, ArXiv e-prints
Oliver S. et al., 2010, MNRAS, 405, 2279
Pacifici C., Kassin S. A., Weiner B., Charlot S., Gardner J. P., 2013, ApJ, 762, L15
Pannella M. et al., 2009, ApJ, 698, L116
Peng Y.-j. et al., 2010, ApJ, 721, 193
Reddy N. A., Pettini M., Steidel C. C., Shapley A. E., Erb D. K., Law D. R., 2012, ApJ, 754, 25
Renzini A., 2009, MNRAS, 398, L58
Rodighiero G. et al., 2010, A&A, 518, L25
Rodighiero G. et al., 2011, ApJ, 739, L40
Ruiz A. N. et al., 2013, ArXiv e-prints
Salim S. et al., 2007, ApJS, 173, 267
Santini P. et al., 2009, A&A, 504, 751
Santini P. et al., 2012, A&A, 538, A33
Sargent M. T., Béthermin M., Daddi E., Elbaz D., 2012, ApJ, 747, L31
Sawicki M., 2012, MNRAS, 421, 2187
Somerville R. S., Hopkins P. F., Cox T. J., Robertson B. E., Hernquist L., 2008, MNRAS, 391, 481
Springel V. et al., 2005, Nature, 435, 629
Stark D. P., Schenker M. A., Ellis R., Robertson B., McLure R., Dunlop J., 2013, ApJ, 763, 129
Stinson G. S., Brook C., Macciò A. V., Wadsley J., Quinn T. R., Couchman H. M. P., 2013, MNRAS, 428, 129
Stringer M., Cole S., Frenk C. S., Stark D. P., 2011, MNRAS, 414, 1927
Tomczak A. R. et al., 2014, ApJ, 783, 85
Torrey P., Vogelsberger M., Genel S., Sijacki D., Springel V., Hernquist L., 2014, MNRAS, 438, 1985
Trujillo-Gomez S., Klypin A., Colin P., Ceverino D., Arraki K., Primack J., 2013, ArXiv e-prints
Wang L. et al., 2013, MNRAS, 431, 648
Weinmann S. M., Pasquali A., Oppenheimer B. D., Finlator K., Mendel J. T., Crain R. A., Macciò A. V., 2012, MNRAS, 426, 2797
Whitaker K. E. et al., 2011, ApJ, 735, 86
Whitaker K. E., van Dokkum P. G., Brammer G., Franx M., 2012, ApJ, 754, L29
Williams R. J., Quadri R. F., Franx M., van Dokkum P., Labbé I., 2009, ApJ, 691, 1879
Wuyts S. et al., 2007, ApJ, 655, 51
Yang X., Mo H. J., van den Bosch F. C., Bonaca A., Li S., Lu Y., Lu Y., Lu Z., 2013, ApJ, 770, 115
York D. G. et al., 2000, AJ, 120, 1579

APPENDIX A: INFERRING THE STELLAR MASS ASSEMBLY HISTORIES OF STAR FORMING GALAXIES

This appendix introduces the main sequence integration (MSI) technique as a method of inferring the average stellar mass assembly histories of star forming galaxies. We then present a discussion of testing the technique by attempting to recover the stellar mass assembly histories predicted by GALFORM. Finally, details of the observational compilation used to infer the stellar mass assembly

histories of star forming galaxies and a discussion of the results is provided.

A1 Main sequence integration

The underlying idea of MSI is that an "average" galaxy can be tracked across the star formation rate versus stellar mass plane by using measurements of the average star formation rate, at a given stellar mass and lookback time, for galaxies which belong to a star forming sequence. This evolutionary track is then integrated, either forwards or backwards in time, from a specified starting mass, $M_\star(t_0)$, and starting time, t_0. For the case of integrating backwards in time, the resulting stellar mass assembly history is given by

$$M_\star(t) = M_\star(t_0) - \int_t^{t_0} \langle \psi(M_\star, t') \rangle \, \mathrm{d}t' + \int_0^{t_0} \langle \psi(M_\star, t') \rangle \, R(t_0 - t') \, \mathrm{d}t' - \int_0^{t} \langle \psi(M_\star, t') \rangle \, R(t - t') \, \mathrm{d}t', \quad \text{(A1)}$$

where $\langle \psi(M_\star, t) \rangle$ is the average star formation rate of star forming galaxies of stellar mass $M_\star$ at time t and $R(t)$ is the fraction of mass returned to the ISM by SNe and stellar winds for a simple stellar population of age t. For the case of integrating backwards in time, this equation can only be solved numerically using an iterative method in order to account for the returned fraction (see Leitner & Kravtsov 2011)). For this study, we instead choose to be consistent with the approach used in GALFORM by adopting the instantaneous recycling approximation. In this case, $R(t)$ is replaced by a constant (set to 0.39 to be consistent with our fiducial GALFORM model) and Equation A1 simplifies to

$$M_\star(t) = M_\star(t_0) - (1 - R) \int_t^{t_0} \langle \psi(M_\star, t') \rangle \, \mathrm{d}t', \quad \text{(A2)}$$

which can be solved numerically using a simple Runge-Kutta integration scheme. The effect of assuming instantaneous recycling can be seen by examining Fig. 9 in Leitner (2012). Relative to the other uncertainties on the inferred stellar mass assembly histories which we discuss later, we expect from their Fig. 9 that the effect of assuming instantaneous recycling is most likely negligible.

In order to calculate $M_\star(t)$ using Equation A2 at each timestep, the average star formation rate of star forming galaxies, $\langle \psi(M_\star, t) \rangle$, must be specified using measurements of the star forming sequence. Our parametrisation of $\langle \psi(M_\star, t) \rangle$ is described in Appendix A2 for our application to GALFORM, and in Appendix A3 for our application to a compilation of observational data. Finally, for a more intuitive link to the dark matter halo mass assembly histories which we consider later, we choose to work in terms of stellar mass assembly histories rather than star formation histories. As we assume instantaneous recycling, both in the model and when analysing the observational data, these are related trivially by linking the stellar mass assembly rate, $\dot{M}_\star$, to the star formation rate using $\dot{M}_\star = (1 - R) \, \psi(M_\star, t)$.

A2 Stellar mass assembly histories of GALFORM galaxies and validation of MSI

In Fig. A1 we show the average stellar mass assembly histories of galaxies from our fiducial GALFORM model that are central and star forming at $z = 0$. The solid blue lines in Fig. A1 show the mean stellar mass assembly histories taken directly from our fiducial model. It can be seen that, roughly speaking, the overall shape of the mass assembly histories is nearly independent of the final stellar mass. Each stellar mass bin shows a sharp rise at early times before flattening out over the majority of the age of the universe. There is a slight deviation from this behaviour for galaxies with $M_\star(t_0) \approx 10^{11} \, \mathrm{M}_\odot$, which instead display a gradual decline in the stellar mass assembly rate after a peak at $t_{\mathrm{lb}} \approx 11 \, \mathrm{Gyr}$. The dashed blue lines in Fig. A1 show the 10^{th}, median and 90^{th} percentiles, indicating the spread in the distribution around the mean.

As well as using the MSI technique to compare these model predictions with any trends inferred from observational data, it is useful to test how well the MSI technique works when applied to the star forming sequence predicted by our fiducial model. To apply MSI to GALFORM, it is necessary to first specify the form of the star forming sequence in the model by parametrising $\langle \psi(M_\star, t) \rangle$. In principle, we could tabulate this for all of the output times used to generate the assembly histories shown in Fig. A1. However, to serve as a fairer comparison to the case where MSI is applied to observational data, we instead choose a simple parametric form for $\psi(M_\star, t)$ given by

$$\frac{\langle \psi(M_\star, t) \rangle}{\mathrm{M}_\odot \mathrm{Gyr}^{-1}} = 10^{11} \left(\frac{c(t)}{\mathrm{Gyr}^{-1}} \right) \left(\frac{M_\star}{10^{11} \, \mathrm{M}_\odot} \right)^{1 + \beta_{\mathrm{sf}}}, \quad \text{(A3)}$$

where β_{sf} is the power-law slope of the star forming sequence which is assumed to be constant with time. $c(t)$ specifies the evolution in the normalisation of the star forming sequence. We find that a reasonable parametrisation for the normalisation is given by fitting a power law of the form

$$c(t) = 0.95 \, (1 + z)^{1.23} \, \mathrm{Gyr}^{-1}. \quad \text{(A4)}$$

We note that this simple parametrisation of $\langle \psi(M_\star, t) \rangle$ is clearly an oversimplification given that the predicted power-law slope, β_{sf}, of the sequence shown in Fig. 1 and Fig. 2 steepens with redshift. However, the slope inferred from the observational data described in Appendix A3 is not sufficiently well constrained with regard to showing a convincing evolution with redshift. Therefore, for the purposes of making a fair assessment of the MSI technique when applied to observational data, we choose to keep β_{sf} as constant in time.

The result of applying MSI to our fiducial GALFORM model can be seen by comparing the blue (intrinsic) and green (inferred from MSI) lines in Fig. A1. The agreement is not perfect. However, it can be seen that MSI broadly reproduces the flat shape of the stellar mass assembly histories predicted by our fiducial model. The worst agreement is seen for the $\log(M_\star(t_0)/\mathrm{M}_\odot) = 8.5$ bin, where MSI predicts that the mass assembly rate should steadily rise from early times up to $z = 0$. In addition, our application of MSI slightly underpredicts the mass assembly rates of the most massive galaxies, such that the predicted stellar mass assembly histories do not drop correctly at early times.

We now consider several potential shortcomings of the MSI technique that could all contribute to this disagreement. Firstly, MSI assumes that star forming galaxies at a given point in time have always been on the star forming sequence prior to that time. We showed in Fig. 1 that there is a tight star forming sequence predicted by our fiducial model. However, in principle it is possible that galaxies could be quenched (for example by a major merger triggered starburst event using up all the cold gas) before accreting

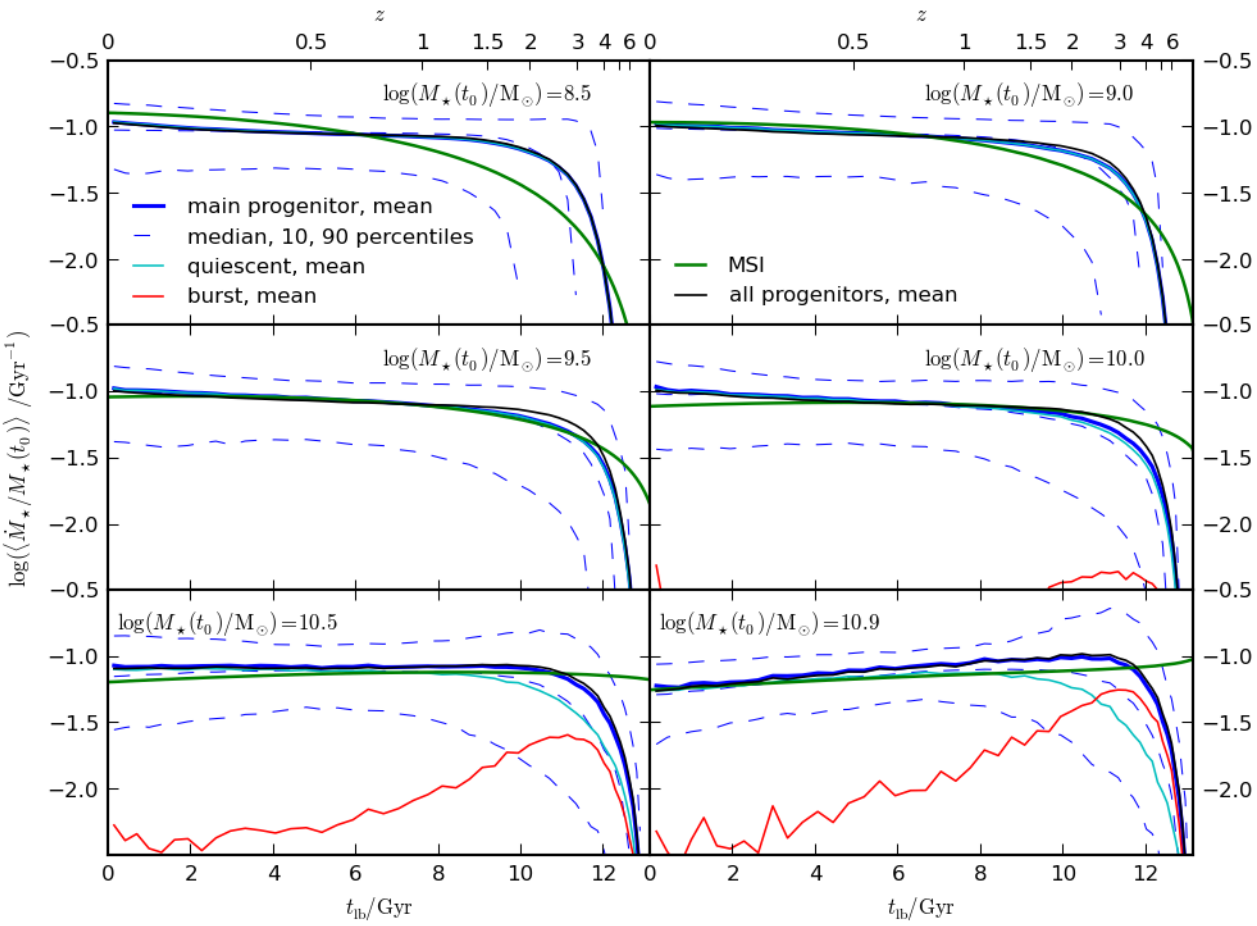

Figure A1. The average stellar mass assembly histories from our fiducial GALFORM model of central galaxies that are star forming at $z = 0$, plotted as a function of lookback time. Model galaxies are binned by their stellar mass at $z = 0$, with each panel corresponding to a different mass bin. The median $z = 0$ stellar mass in each bin is labelled in each panel. Heavy blue solid lines show the mean stellar mass assembly histories for the main stellar progenitors, as calculated directly from our fiducial model. Dashed blue lines show the corresponding 10^{th}, median and 90^{th} percentiles of the distribution. Cyan and red lines show, respectively, the contribution to the mass assembly histories from quiescent star formation and bursts. Black lines show the mean stellar mass assembly histories but for the case of summing over all of the stellar progenitors of each $z = 0$ galaxy. These are largely coincident with the heavy blue lines. Green lines show the stellar mass assembly histories calculated by applying the MSI technique to the star forming sequence predicted by our fiducial model.

enough fresh gas onto a disk to rejoin the star forming sequence. The impact from such a scenario can be tested in a straightforward manner by considering the dispersion in the distribution of mass assembly rates around the mean, as shown in Fig. A1. We find that the typical dispersion is roughly compatible with the dispersion at a given stellar mass of the star forming sequence shown in Fig. 1. This supports, in a statistical sense, the assumption folded into the MSI technique that galaxies which are star forming at $z = 0$ do not drop below the sequence at some earlier stage in their evolution, at least for a significant period of time.

A second potential shortcoming of the MSI technique is that it ignores the hierarchical assembly of stellar mass through galaxy merging events. It is possible that a significant fraction of the stellar mass of a star forming galaxy at $z = 0$ was formed in multiple progenitors, in which case the MSI method breaks down unless the sum of these progenitors also conspires to reside on the star forming sequence. We check for the contribution from merging by comparing the mean stellar mass assembly histories of the main stellar progenitors (solid blue lines) to the sum of all stellar progenitors (black lines) in Fig. A1. Over all of the stellar mass bins considered, it can be seen from Fig. A1 that the stellar mass assembly histories of galaxies that are central and still star forming at $z = 0$ are dominated by the main stellar progenitor, providing support for the validity of the MSI technique. This result is perhaps unsurprising, in that in order for the stellar mass of a secondary progenitor to become significant relative to the stellar mass of the main progenitor, the system must undergo a major merging event which would ultimately quench star formation in the resulting galaxy as gas is used up in a starburst event.

To emphasise the difference between the star forming galaxy population we consider here and passive galaxies, we show in Fig. A2 the average stellar mass assembly histories of model galaxies that are central and passive at $z = 0$. In contrast to Fig. A1, the stellar mass assembly histories of the main progenitors of passive centrals (blue lines) are significantly different from the stellar mass assembly histories obtained from summing over all progenitors (black lines). This difference is largest for the most massive galaxies where a significant amount of stellar mass is assembled

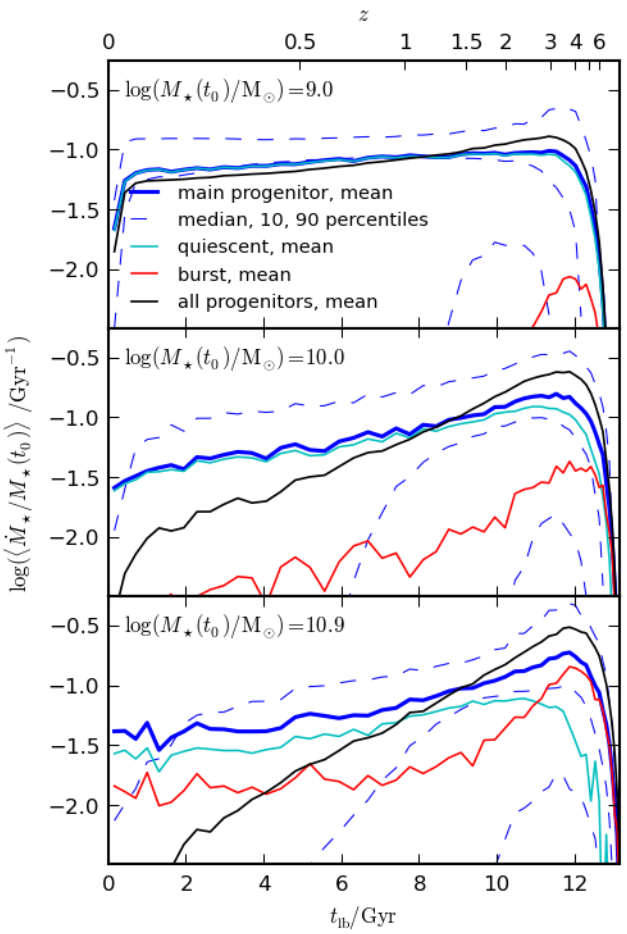

Figure A2. The average stellar mass assembly histories of central galaxies that are passive at $z = 0$ from our fiducial GALFORM model, plotted as a function of lookback time. Model galaxies are binned by their stellar mass at $z = 0$, with each panel corresponding to a different mass bin. The median $z = 0$ stellar mass in each bin is labelled in each panel. The meaning of the lines is the same as for Fig. A1.

in secondary progenitors at early times which merge onto the main progenitor galaxy later. The blue lines also include the rate of accretion of stellar mass from secondary progenitors and can therefore exceed the black lines in this case.

Returning to the star forming galaxy sample, Fig. A1 also shows that quiescent star formation (cyan lines) mostly dominates the stellar mass assembly rates of galaxies which are still star forming at $z = 0$, as compared to star formation in bursts (red lines). The only exception to this is for the progenitors of massive star forming galaxies at $z = 0$, where bursts briefly dominate the stellar mass assembly process at high redshift. Integrated over the lifetime of these galaxies however, the burst star formation mode is still entirely subdominant. This is important for the MSI technique because bursts can perturb galaxies above the star forming sequence. However, as has also been shown by Lamastra et al. (2013), we find that actively bursting galaxies in hierarchical galaxy formation models can also reside on (or in same cases below) the star forming sequence. As an aside, the result that star formation in the galaxies considered in Fig. A1 is dominated by quiescent star formation in the main stellar progenitor lends support to the methodology employed by galaxy formation models which ignore galaxy merging and disk instabilities, provided that these models are used only to predict the statistical properties of actively star forming central galaxies (e.g. Dutton et al. 2010).

Finally, it should be noted that the MSI technique which we employ for this study includes the assumption that the star forming sequence can be described by a single, unbroken power law over all relevant scales in stellar mass. Fig. 2 shows that this is only approximately true for the star forming sequence in our fiducial GALFORM model. If the true star forming sequence cannot be adequately described by a single power law then the resulting stellar mass assembly histories inferred using the MSI technique will be in error. As we start the integration process at $z = 0$, this error would become more severe at early times. In addition, as noted earlier, Fig. 2 shows that the power-law slope of the star forming sequence, $\beta_{\rm sf}$, evolves with redshift in our fiducial model. Comparison of the true (solid blue) and inferred (green) average stellar mass assembly histories in Fig. A1 shows that MSI does not perfectly agree with the direct model prediction, and that the disagreement becomes worse at early times. Given that the other potential sources of error which we have considered until now appear to be insignificant, we attribute the disagreement between MSI and the direct model output seen in Fig. A1 to the simple power-law parametrisation of $\langle\psi(M_\star, t)\rangle$ which we use to perform MSI. Given these problems, any comparison between MSI and direct model predictions should only be interpreted taking into account that the MSI technique likely fails to precisely constrain the shape of the stellar mass assembly histories of galaxies, particularly at early times. Nonetheless, the qualitative trend of almost flat stellar mass assembly histories seen in Fig. A1 is broadly reproduced by the MSI technique for all but the least massive galaxies. We can therefore proceed to perform a qualitative comparison between the shapes of the stellar mass assembly histories predicted by our model and those inferred from observational data using MSI.

A3 Applying main sequence integration to observational data

To infer the average stellar mass assembly histories of galaxies from observations using the MSI technique, it is necessary to specify $\langle\psi(M_\star, t)\rangle$ for all possible values of $M_\star$ and t. Rather than attempt to interpolate directly between the observational data on the average specific star formation rates presented in Section 3.3, we instead choose to first compile a list of power-law fits to the star forming sequence for different redshifts from the literature. Basic information on this compilation is presented in Table A1. Using Equation A3, we parametrise these power-law fits with the slope, $\beta_{\rm sf}$ and the normalisation, $c(t)$. We convert the fits taken from studies that assume a Salpeter IMF to a Chabrier IMF by applying a correction of -0.24 dex to both ψ and $M_\star$ (Ilbert et al. 2010; Mitchell et al. 2013). This typically makes only a very small difference to the resulting power-law fits.

We show our observational compilation of $\beta_{\rm sf}$ as a function of lookback time in Fig. A3. This shows that currently there is not a strong consensus on the slope of the star forming sequence in the literature. Given the wide range of selection techniques that are used to separate star forming galaxies, we expect the variation in $\beta_{\rm sf}$ seen in Fig. A3 to be driven primarily by selection effects. For example, Karim et al. (2011) explore this issue in an appendix and show that increasingly blue rest-frame $(NUV - r)$ colour cuts result in increased values of $\beta_{\rm sf}$. Another issue is whether the star forming sequence can really be described by a single unbroken power law in $M_\star$ (see Huang et al. 2012). For example, if the slope

Source	Redshift	Selection	SF cut	Tracer	Symbol
Daddi et al. (2007)	1.4-2.5	BzK	sBzK	UV (corrected)	×
Elbaz et al. (2007)	0.8-1.2	z	blue colour	24μm+UV	×
Salim et al. (2007)	0.05-0.2	r	BPT diagram	SED fitting	×
Santini et al. (2009)	0.3-2.5	K_s	SFR-$M_\star$ distribution	24μm+UV	♦
Labbé et al. (2010)	7	LBG	blue colour	UV (corrected)	■
Oliver et al. (2010)	0-2	Optical	template fitting	70/160μm	♦
Peng et al. (2010)	0-1	Optical	blue colour	SED fitting	×
Rodighiero et al. (2010)	0-2.5	4.5μm	blue colour/24μm detection	FIR	★
Elbaz et al. (2011)	0-3	24μm	24μm detection	FIR	▶
Karim et al. (2011)	0.2-3	3.6μm	blue colour	Radio	•, •
Bouwens et al. (2012)	4	LBG	blue colour	UV (corrected)	+
Lin et al. (2012)	1.8-2.2	BzK	sBzK	UV (corrected)	▲
Reddy et al. (2012)	1.4-3.7	LBG	blue colour	24μm+UV	+
Sawicki (2012)	2.3	UV	blue colour	UV (corrected)	■
Whitaker et al. (2012)	0-2.5	K	(U-V/V-J) cut	24μm+UV	+
Koyama et al. (2013)	0.4,0.8,2.2	H_α	H_α	H_α (corrected)	♦
Wang et al. (2013)	0.2-2	K	SFR-$M_\star$ distribution	SED fitting / FIR	■

Table A1. List of the sources of power-law fits to the observed star forming sequence extracted from the literature. We list the source, redshift range or median redshift, galaxy selection technique, the subsequent star forming galaxy selection technique, and the tracer used to estimate the instantaneous star formation rate. The symbols used for each source in Fig. A3 and Fig. A4 are also shown. For LBG selected samples, it should be noted that the initial galaxy selection technique is strongly biased towards blue star forming galaxies, so typically no additional cut to separate star forming galaxies is performed. For Karim et al. (2011), we use both the star forming galaxy sample presented in their Table 3 as well as the active population which is shown in their Figure 13 (which uses a bluer colour cut). The code and observational data used for this compilation are available at `http://www.astro.dur.ac.uk/~d72fqv/MS_fits/`.

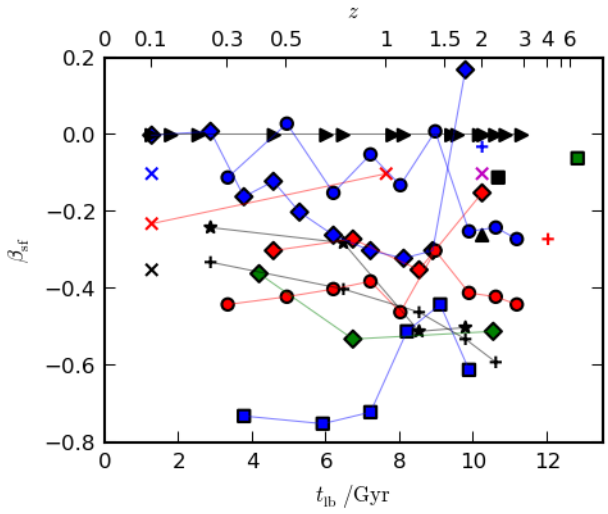

Figure A3. The slope of power-law fits to the observed star forming sequence from the literature, plotted as a function of lookback time. Each symbol corresponds to data from a different source. The list of sources for the compilation is presented in Table A1, which also references which source matches a given symbol.

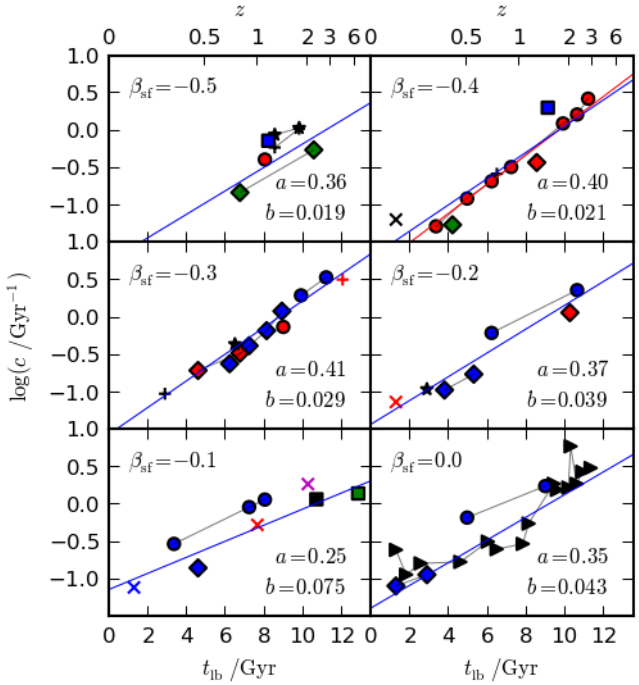

Figure A4. Normalisation of power-law fits to the star forming sequence from the literature, plotted as a function of lookback time. The list of sources for the compilation is presented in Table A1, which also references which source matches a given symbol. Each panel shows the normalisation for different bins of the fitted power-law slope to the star forming sequence, β_{sf}, as labelled. For each panel, the evolution of the normalisation is fitted by $(c/\mathrm{Gyr}^{-1}) = b\,\exp(a\,t_{lb}/\mathrm{Gyr})$ and the best fitting a and b are labelled. These fits are shown as blue lines and use all of the observational data, including data from Karim et al. (2011). In addition, we also perform an independent fit (red line) to just the Karim et al. (2011) star forming sample (red circles) in isolation for the $\beta_{sf} = -0.4$ bin.

of the sequence changes at the high mass end then the range in stellar mass probed by each individual study will have an effect on the inferred slopes. Inspection of Fig. 2 shows evidence that this does indeed occur in our fiducial model.

Given this uncertainty in the true slope of the star forming sequence, we first make the simplest possible assumption, which is that the slope remains constant with lookback time. We then choose to estimate $\langle\psi(M_\star, t)\rangle$ by first binning the power-law fits from Table A1 in β_{sf}, before performing a fit to $c(t)$ for each bin as a function of lookback time. For two of the studies included in our compilation (Lin et al. 2012; Reddy et al. 2012), a best fitting slope to the

star forming sequence is provided but the corresponding normalisation is not available, and so they do not appear in Fig. A4 or feature in the following fits. The resulting data and fits to the evolution in the normalisation are shown in Fig. A4.

Unlike the slope, there is actually a reasonable consensus in the literature on the evolution in $c(t)$ for a given $\beta_{\rm sf}$ bin. We find that the evolution in the normalisation seen in Fig. A4 is best fit as an exponential function of lookback time rather than as a power law in $(1+z)$. We therefore parametrise the evolution in the normalisation using

$$\frac{c(t)}{\mathrm{Gyr}^{-1}} = b\,\exp\left(a\,\frac{t_{\rm lb}}{\mathrm{Gyr}}\right). \quad \text{(A5)}$$

To account for the oversampling in the number of points at $z \approx 2$ in some of the $\beta_{\rm sf}$ bins, we weight all the points shown in Fig. A4 to give equal weight to each bin in $\Delta t_{\rm lb} = 1\,\mathrm{Gyr}$ within each panel. In order to facilitate a qualitative comparison with the method used by Leitner (2012) to estimate the star formation histories of star forming galaxies, we also perform an independent fit to the star forming galaxy sample from Karim et al. (2011), fixing $\beta_{\rm sf} = -0.4$. This fit to the evolution in the normalisation, $c(t)$, is shown by the red line in Fig. A4.

Once $\langle\psi(M_\star,t)\rangle$ has been parametrised, we can apply MSI to infer the average stellar mass assembly histories of $z=0$ star forming galaxies for different values of the stellar mass at $z=0$, $M_\star(t_0)$. The results of this exercise are shown as coloured lines in Fig. A5, with each line corresponding to a different bin in $\beta_{\rm sf}$. To compare with the approach used by Leitner (2012), we also apply MSI to only the star forming sample presented in Karim et al. (2011). The results of doing this are shown by the dashed black curves in Fig. A5.

It is immediately apparent that the uncertainty on the slope of the star forming sequence reported in the literature translates to a considerable uncertainty on the stellar mass assembly histories inferred from the data. The uncertainty is largest for low mass galaxies where, in particular, the formation time at which a given galaxy forms a given fraction of its stars is very poorly constrained. This partly reflects the fact that an increasingly large extrapolation in $\langle\psi(M_\star,t)\rangle$ has to be made for smaller galaxies as the stellar mass of their progenitors typically drops below the completeness limit of the observational surveys used to obtain $\langle\psi(M_\star,t)\rangle$.

Despite the considerable uncertainties, qualitatively the data seems to favour a scenario where galaxies that are still star forming at $z=0$ undergo a peak phase of star formation activity at $z \approx 1$, followed by a drop towards late times. The actual position of the peak and the rate of late time decline are somewhat poorly constrained. Furthermore, for $\beta_{\rm sf} < -0.2$, the position of this peak clearly depends on $M_\star(t_0)$, such that a downsizing trend is apparent. Massive star forming galaxies are inferred to form a greater fraction of their stellar mass at early times compared to lower mass galaxies in this case. This is the conclusion presented in Leitner (2012) who use only data from Oliver et al. (2010) and the star forming sample from Karim et al. (2011) as inputs to their application of MSI. Such a downsizing trend, provided that star forming galaxies are successfully separated from passive galaxies, should be completely independent of any physical processes that cause permanent quenching of star formation. On the other hand, if $\beta_{\rm sf}$ is larger, then the shapes of the stellar mass assembly histories of galaxies that are star forming at $z=0$ are almost completely independent of their final stellar mass.

The stellar mass assembly histories inferred from applying MSI to only the star forming sample presented in Karim et al. (2011) (dashed black lines) are mostly consistent with the curves obtained by fitting to data taken from the entire observational compilation. This implies that the approach used by Leitner (2012), which relies primarily on the Karim et al. (2011) data, should yield results that are consistent with ours. On the other hand, it can be seen from the red line shown in Fig. A4 that extrapolating the Karim et al. (2011) results down to $z=0$ favour a steeper late time drop in the normalisation of the star forming sequence than is implied by SDSS data (Salim et al. 2007). This is reflected in the steeper drop in the stellar mass assembly histories inferred from applying MSI to only the Karim et al. (2011) data in Fig. A5. This emphasises the need to consider results from as much of the literature as possible in order to try to account for the considerable uncertainties on the slope and normalisation of the star forming sequence.

APPENDIX B: INVARIANCE IN THE SHAPE OF PREDICTED STELLAR MASS ASSEMBLY HISTORIES

In Section 4.1, we demonstrated that, qualitatively, the stellar mass assembly histories predicted by our fiducial GALFORM model do not agree closely with the trends we infer from observational data. In this appendix, we address the fact that our fiducial model is only one specific realisation of GALFORM with regard to the various model parameters that can be changed. These parameters are constrained by matching global diagnostics of the galaxy population. We now proceed to demonstrate that the disagreement between GALFORM and the observational data holds for a wide range of choices of these model parameters. This result stems from our finding that the shapes of the average stellar mass assembly histories of central star forming galaxies in GALFORM are almost entirely invariant when changing model parameters relating to star formation, feedback and gas reincorporation.

We demonstrate this behaviour in Fig. B1, which shows the average stellar mass and halo mass assembly histories of model galaxies which are central and star forming at $z=0$. We show the output of a variety of variants of our fiducial model. These variants are chosen as examples to display the range of mass assembly histories which arise as a result of changing various model parameters in GALFORM which are relevant to star forming galaxies. Included are parameters that control the global efficiency of star formation and SNe feedback, the gas reincorporation timescale and the dependence of the mass loading factor, β, on the circular velocity of galaxies. Note that it is possible, in principle, that changing these model parameters would affect the position of the star forming sequence in GALFORM, invalidating our separation between star forming and passive galaxies. We have verified that this is, in fact, not the case and find that the star forming galaxy cuts shown as blue lines in Fig. 1 continue to be effective at isolating the star forming sequence for all the models and redshifts considered here.

To first order, the stellar mass assembly histories for all the models shown in Fig. B1 are almost identical for a given stellar mass, $M_\star(t_0)$, with significant variations only occurring at early times. In contrast, the normalisation of the halo mass assembly histories shifts significantly between different choices of model parameters. Therefore, while these model parameters in GALFORM are capable of changing the $z=0$ stellar mass function by changing the relationship between stellar mass and halo mass, they do

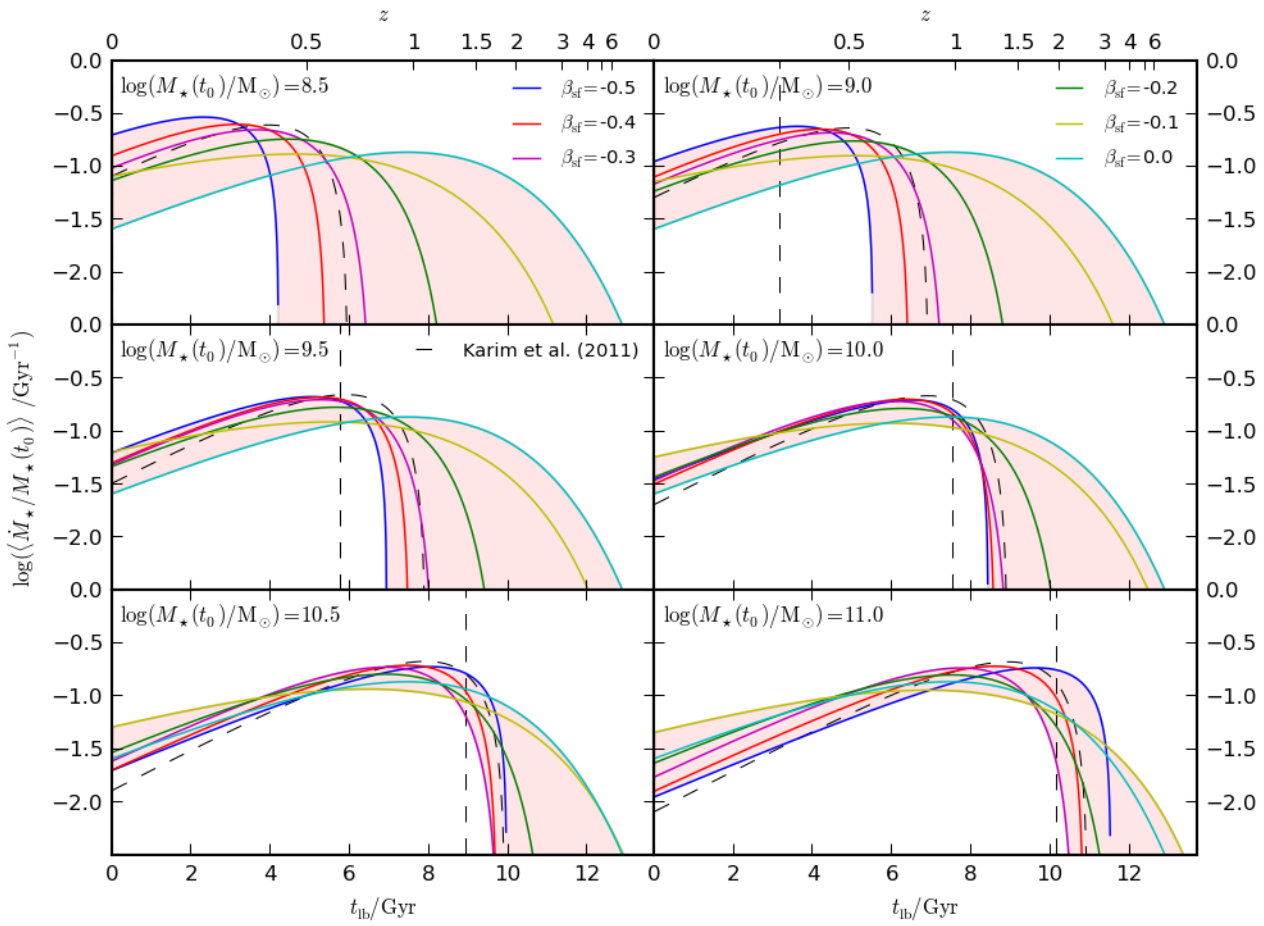

Figure A5. The stellar mass assembly histories of star forming galaxies inferred by applying MSI to observational data, plotted as a function of lookback time. Each panel corresponds to a different $z = 0$ stellar mass, as labelled. Coloured solid lines show the mass assembly histories inferred by applying MSI to the observational compilation presented in Table A1. Each solid line in a given panel corresponds to a different bin in the power-law slope of the star forming sequence, $\beta_{\rm sf}$, as taken from the compilation. Dashed black curves show the mass assembly histories inferred by applying MSI to the star forming galaxy sample from Karim et al. (2011). The dashed vertical lines show the lookback time beyond which the MSI technique, applied to the Karim et al. (2011) sample, extrapolates below the stellar mass completeness limits of Karim et al. (2011). For the $\log(M_\star(t_0)\,/{\rm M}_\odot) = 8.5$ panel, the entire stellar mass assembly history inferred from Karim et al. (2011) involves an extrapolation below this mass completeness limit.

not significantly affect the stellar mass assembly process of central galaxies of a given stellar mass at $z = 0$.

This result can be understood by first reviewing the way that the stellar mass assembly process takes place in GALFORM. As discussed in, for example, Fakhouri et al. (2010), the specific halo mass assembly rate and consequently the shape of the corresponding dark matter halo mass assembly histories are nearly independent of the final halo mass (see their Equation 2). This can be seen directly in Fig. B1. Secondly, as shown in Section 4.1, stellar mass assembly broadly tracks halo mass assembly in our fiducial GALFORM model. As described in Section 4.2, this coevolution arises because the mass loading and reincorporation efficiencies do not evolve significantly over the majority of the lifetimes of typical star forming galaxies. For the parametrisations currently used to model these physical processes in GALFORM, changing the relevant model parameters merely changes their efficiency in a global sense. Therefore, in order to change the shape of the stellar mass assembly histories, an alternative parametrisation of one (or both) of these processes would be required. Such a modification would need to result in significantly stronger evolution in the mass loading factor, $\beta_{\rm ml}$, or the reincorporation timescale, $t_{\rm ret}$, than is seen for our fiducial model in Fig. 6.

APPENDIX C: VIRIAL MASS SCALING MODEL

In Section 5.2, we demonstrate that by modifying the reincorporation timescale in the model to the form given by Eqn 25, it is possible to reconcile the predicted and inferred stellar mass assembly histories of galaxies that are still star forming at $z = 0$. In Fig. 8 we show that this ad hoc model for the reincorporation timescale is quite different from the modification introduced by Henriques et al. (2013) in order to reproduce the observed evolution of the stellar mass and luminosity functions. We now consider implementing into our model their suggestion that the reincorporation timescale should only scale with the halo virial mass as

$$t_{\rm ret} = \gamma \frac{10^{10}{\rm M}_\odot}{M_{\rm H}}. \qquad \text{(C1)}$$

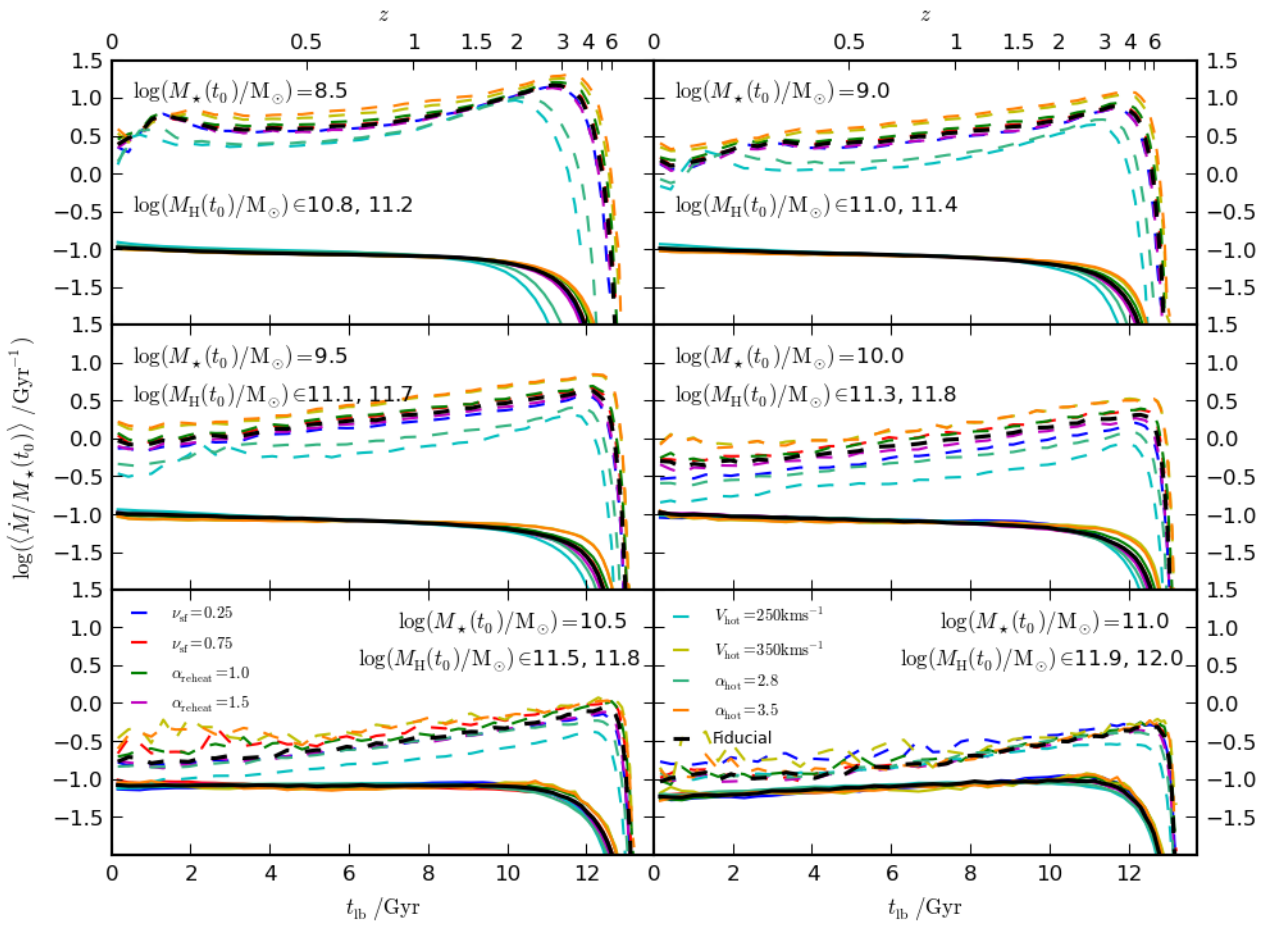

Figure B1. The mean mass assembly histories of model central galaxies that are star forming at $z = 0$, plotted as a function of lookback time. Solid lines show predictions for the mean stellar mass assembly histories of the main stellar progenitors of galaxies. Black lines correspond to our fiducial GALFORM model. Other colours correspond to variations of our fiducial model, with a single model parameter changed to the labelled value. Definitions of these model parameters can be found in Section 2.1. Dashed lines show the corresponding dark matter halo mass assembly histories of the progenitor haloes that host the main stellar progenitors of central star forming galaxies at $z = 0$. The halo mass assembly curves are rescaled by $\Omega_{\rm b}/\Omega_{\rm M}$ to show the baryonic accretion rate onto these haloes. Model galaxies are binned according to their $z = 0$ stellar mass with each panel corresponding to a different mass bin. The median $z = 0$ stellar mass in each bin is labelled in each panel. The range (across all of the GALFORM models shown) in the corresponding median $z = 0$ dark matter halo mass of each stellar mass bin is also labelled.

We start by requiring that this virial mass scaling model should provide an adequate match to the $z = 0$ stellar mass function. Starting from our fiducial model, we find that it is possible to do this simply by implementing Eqn C1 with γ changed from 18 Gyr, as in Henriques et al. (2013), to 5.6 Gyr.

Comparisons with the other models considered in this paper for the evolution in the specific star formation rates and stellar mass assembly histories of star forming galaxies are shown in Fig. 3 and Fig. 9 respectively. Fig. 9 shows that the virial mass scaling model predicts rapidly rising stellar mass assembly histories for all but the most massive star forming galaxies at $z = 0$. For galaxies with $\log(M_\star/{\rm M}_\odot) = 10$ at $z = 0$, this results in dramatic disagreement with the stellar mass assembly histories inferred from observations with too much star formation at late times compared to early times. For low mass galaxies, the observational constraints are very weak, such that any model could be compatible. For the most massive systems, we note that similar to the modified reincorporation model shown in red, the cooling timescale in the virial mass scaling model becomes long compared the reincorporation timescale for galaxies residing within massive haloes. As discussed in Section 5.2, modifying the reincorporation timescale in this regime will have a much smaller impact as the gas cycle becomes limited by cooling. Fig. 3 shows that the virial mass scaling model predicts specific star formation rate evolution which is too slow at a fixed stellar mass relative to the rapid evolution inferred from observations. Again, the specific star formation rates of massive star forming galaxies are relatively unaffected by modifications to the reincorporation timescale.

While our modified reincorporation model is more successful than the virial mass scaling model in reproducing the trends inferred from the data in Fig. 3 and Fig. 9, it is important to also consider the predicted evolution of the stellar mass function, given that this is the main constraint used by Henriques et al. (2013). Stellar mass function predictions for the different models considered in this paper are compared to a compilation of observational data in Fig. C1. To first order, the differences between the models can be summarised simply by noting that relative to our fiducial model, the modified reincorporation model suppresses both early and late star

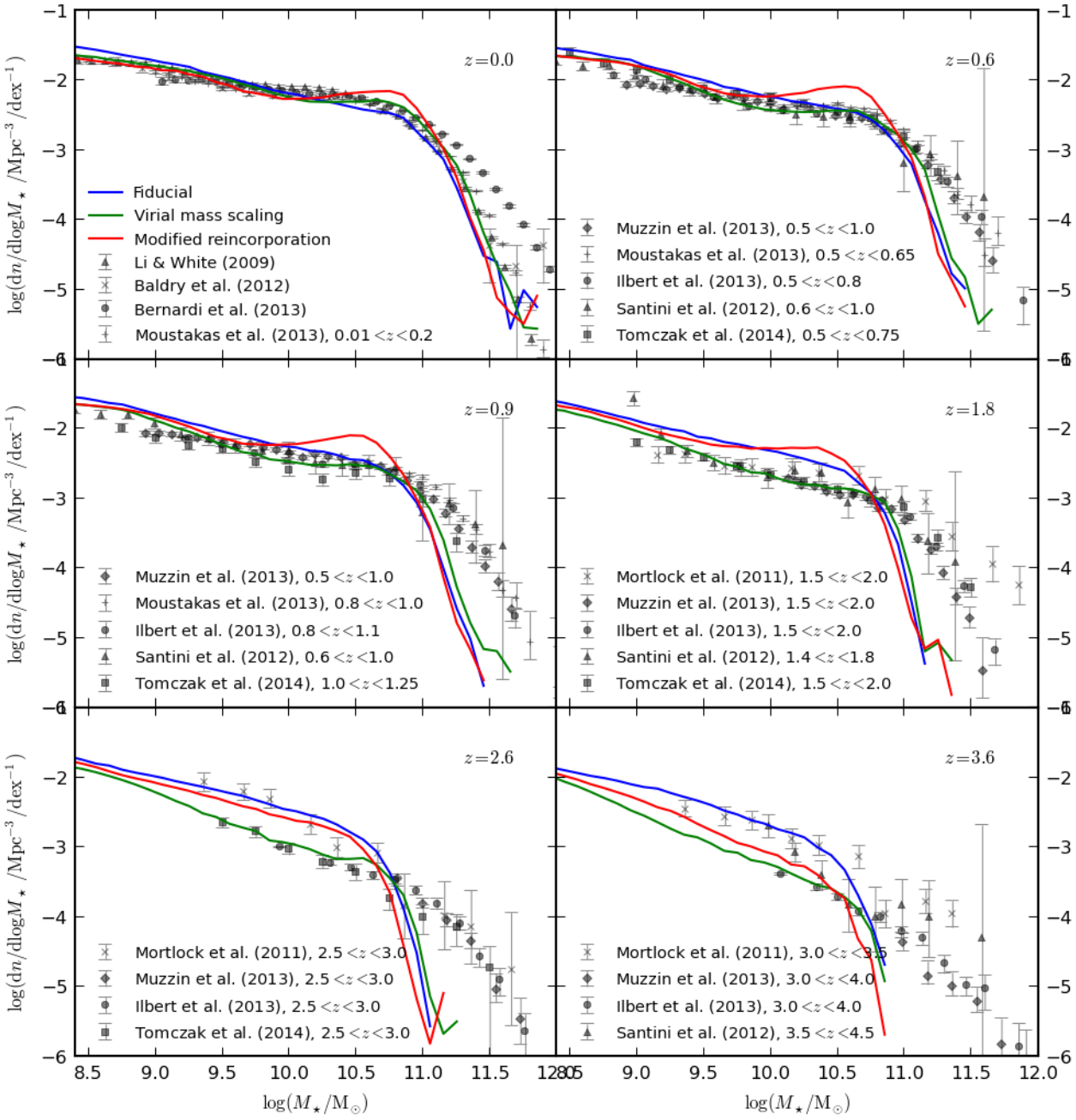
z=0.0
Fiducial
Virial mass scaling
Modified reincorporation
Li & White (2009)
Baldry et al. (2012)
Bernardi et al. (2013)
Moustakas et al. (2013), 0.01 <z<0.2
z=0.6
Muzzin et al. (2013), 0.5 <z<1.0
Moustakas et al. (2013), 0.5 <z<0.65
Ilbert et al. (2013), 0.5 <z<0.8
Santini et al. (2012), 0.6 <z<1.0
Tomczak et al. (2014), 0.5 <z<0.75
z=0.9
Muzzin et al. (2013), 0.5 <z<1.0
Moustakas et al. (2013), 0.8 <z<1.0
Ilbert et al. (2013), 0.8 <z<1.1
Santini et al. (2012), 0.6 <z<1.0
Tomczak et al. (2014), 1.0 <z<1.25
z=1.8
Mortlock et al. (2011), 1.5 <z<2.0
Muzzin et al. (2013), 1.5 <z<2.0
Ilbert et al. (2013), 1.5 <z<2.0
Santini et al. (2012), 1.4 <z<1.8
Tomczak et al. (2014), 1.5 <z<2.0
z=2.6
Mortlock et al. (2011), 2.5 <z<3.0
Muzzin et al. (2013), 2.5 <z<3.0
Ilbert et al. (2013), 2.5 <z<3.0
Tomczak et al. (2014), 2.5 <z<3.0
z=3.6
Mortlock et al. (2011), 3.0 <z<3.5
Muzzin et al. (2013), 3.0 <z<4.0
Ilbert et al. (2013), 3.0 <z<4.0
Santini et al. (2012), 3.5 <z<4.5
log(dn/dlogM⋆ /Mpc⁻³ /dex⁻¹)
log(M⋆/M⊙)

Figure C1. Stellar mass functions predicted by the different GALFORM models for a selection of redshifts, as labelled in each panel. Blue lines show predictions from our fiducial model. Red lines correspond to the modified reincorporation model introduced in Section 5.2. Green lines correspond to a model using the virial mass scaling for the reincorporation timescale introduced by Henriques et al. (2013). The grey points and error bars show observational estimates of the stellar mass function from Li & White (2009), Baldry et al. (2012), Ilbert et al. (2010), Mortlock et al. (2011), Santini et al. (2012), Bernardi et al. (2013), Ilbert et al. (2013), Moustakas et al. (2013), Muzzin et al. (2013a) and Tomczak et al. (2014). Where necessary we convert these observational results from a Salpeter to a Chabrier IMF using a $-0.24\,\mathrm{dex}$ correction (Ilbert et al. 2010; Mitchell et al. 2013).

formation. The virial mass scaling model also suppresses early star formation but predicts much stronger star formation at late times for all but the most massive galaxies. This results in much stronger evolution in number density short of the break in the mass function below $z = 2$, in good agreement with the most recent observational data. In contrast, our fiducial model predict an overabundance of low mass galaxies relative to the observations beyond the local Universe.

Compared to the observations, all three models shown here all strongly underpredict the abundance of galaxies above the break of the stellar mass function beyond the local Universe. The extreme end of the mass function must always be interpreted with care because of the potential for Eddington bias to artificially boost the population residing in the massive tail of the galaxy stellar mass distribution. On the other hand, the disagreement at the massive end could be related to the problem that all three models suffer from in failing to reproduce the rapid evolution in the specific star formation rates of massive star forming galaxies with $\log(M_\star/\mathrm{M}_\odot) = 11$ seen in Fig. 3.

At this stage, it is tempting to speculate whether it is possible to produce a model that can be consistent with the observed stellar mass function and star formation evolution simultaneously. One possibility that we did not fully explore in this study would be to search for a modified model which introduces a strong downsizing trend into the purely star forming population, such that low mass galaxies form very late, and yielding a star forming sequence with a slope of $\beta_{\mathrm{SF}} \approx -0.4$, compatible with current observations of the star forming sequence. In this case, it might be possible to reproduce the observed evolution in the low mass end of the stellar mass function while also predicting peaked star formation histories for star forming galaxies with $\log(M_\star/\mathrm{M}_\odot) = 10$ at $z = 0$. We defer any further exploration of this issue to a future paper.

Another consideration is that currently it is assumed in our model that all gas which is removed from galaxies by SNe feedback is added to a reservoir instead of being added straight back into the hot halo gas profile. In the case where the reincorporation timescale is of order the halo dynamical time, this is equivalent to assuming that the ejected gas moves in a ballistic fashion and escapes the halo virial radius before returning. In contrast, the models presented by Guo et al. (2011) and Henriques et al. (2013) assume that only a fraction of this gas is actually ejected from the halo. The remaining fraction is added back into the halo gas profile and is therefore able to inflow back onto the disk very rapidly when cooling timescales are short. In these models, the fraction of gas that is able to escape the halo is parametrised as a function of the halo circular velocity, V_{vir}, such that a larger fraction of gas is ejected from the haloes of low mass systems. Depending on the set of chosen model parameters, this treatment of the gas affected by SNe feedback could change the $z = 0$ stellar mass range over which a modification to the reincorporation timescale would be effective in changing the stellar mass assembly histories of star forming galaxies. Again, we defer any further exploration in this area to future work.